Mechanics and Modeling of Flow and Bed Evolution in Lateral Separation Eddies

Jonathan M. Nelson and Richard R. McDonald

Abstract

Lateral separation eddies are commonly occurring geomorphic features that play key roles in riverine sediment storage, habitat, and recreation, primarily as a result of the efficient sediment-trapping mechanisms acting along the riverward margins of these features. We present a brief synopsis of the important physical effects that drive sediment trapping in these regions, and describe the development of a flow, sediment-transport, and bed evolution model that incorporates these effects. The flow model is divided into two parts, one of which treats the routing of the flow in a vertically averaged sense, and the other of which treats the vertical structure of the flow with emphasis on the generation of secondary flows. Particular attention is paid to developing a turbulence model that is at once simple, computationally feasible, and physically reasonable. Results of the model are compared to laboratory flow and bed evolution measurements in a simple, rectilinear channel expansion, and to flow measurements made in a natural recirculation eddy in the Colorado River in Grand Canyon. The model yields reasonable predictions for the flow field in both cases, and reproduces the bed evolution observed in the laboratory with good accuracy in terms of both rate and duration of bar growth and equilibrium amplitude of the observed bed evolution.

Introduction

Lateral separation eddies are produced in rivers and streams where the main downstream flow separates from the bank of the channel, producing a recirculating flow region with weak upstream-directed velocities near the channel bank. These features occur in regions of high bank curvature, as are typically associated with local bank irregularities, rapid increases in channel width, or strong planform curvature of the channel. The riverward margin of these features is defined as the temporally-averaged streamline

connecting the point of flow separation at the upstream end of the eddy with the point of reattachment at the downstream extent of the eddy (the so-called "reattachment streamline"). The reattachment point is the location where the temporally averaged flow near the bank changes in direction from upstream to downstream, as shown in Figure 1. The flow along the riverward margin of the eddy is characterized by very strong lateral shears and vortex generation near the separation point, with decreasing lateral shears and gradual dissipation of large scale vortices moving downstream toward the reattachment point.

Lateral separation eddies are extremely efficient traps for sediment and organic material. As a consequence of this and their relatively quiescent flows, eddies provide critical habitat for juvenile fish and other aquatic species. Furthermore, these features provide essential storage areas for fine sediment and appear to play a central role in channel width adjustment. However, despite the importance of these features in riparian ecosystems and fluvial geomorphology, relatively little work has been done to understand the exchange processes between the main channel and lateral separation eddies that act to produce their observed trapping efficiency, or to develop computational models for flow and sedimentation in these important channel features.

The most obvious manifestation of sediment trapping by eddies is the bar deposits typically found within them. As reported in detail by Schmidt et al.[1993], Rubin et al.[1990], and others, sedimentary deposits in lateral separation eddies have a characteristic morphology both on the scale of the bar deposits, and on the scale of the sedimentary structures making up the bars. Provided that sediment is mobilized in the main channel adjacent to the separation eddy, deposits formed within lateral separation eddies are often remarkably similar even for eddies with much different geometries and scales. At least to some extent, this suggests that the basic mechanism governing transfer of sediment from the main channel to the separation eddy dominates the problem regardless of scale.

The relative scale-independence of the eddy trapping mechanism suggests that it must be related in some direct manner to the separation and reattachment process. Noting this and investigating laterally-separating flows experimentally, Nelson[1991] and Nelson et al. [submitted] developed a hypothesis for the

trapping mechanism of lateral separation eddies. Specifically, they suggested that transport from the main river flow into the eddy is produced by the interaction of vortices produced along the riverward margin of the eddy with the riverine boundary layer. This interaction produces net advection of relatively sediment-laden near-bed fluid from the main channel directly into the eddy at depth. This model for the dominant exchange mechanism is in direct contrast to treatments that assume exchange across the reattachment streamline is entirely a product of turbulent diffusion, but it explains the observed bar morphology and the trapping efficiency much better.

In this paper, the sediment exchange mechanism described by Nelson et al. [submitted] is incorporated into a coupled numerical model for flow, sediment transport, and bed evolution in channels with lateral separation eddies. The numerical approach is tested for accuracy against both measured flow data and measured bed evolution data. The model accurately predicts both the flow field and bed evolution measured in lateral separation eddies constructed in the laboratory, and. is also compared to flow measurements made in a natural separation eddy in the Colorado River in Grand Canyon. Finally, the approach is used to discuss the importance of externally applied forcing (e.g., from channel curvature, bathymetric variation in the main channel, or bank irregularity) on the geometry of separation eddies, and the importance of sediment supply to the overall problem is discussed with regard to model applications.

Mechanics of Sediment Trapping in Eddies

In order to motivate the approach taken in the numerical development described below, it is critical to have a clear understanding of the processes that are being treated. In this section, laboratory measurements of flow in lateral separation eddies are used to briefly explain the essential mechanics of the exchange process acting between the eddy and the main river channel, so that the more abstract development presented below will have a clear physical interpretation.

Basic Hypothesis

The simplest and most common way to think of the flow field in a lateral separation eddy is by analogy with the flow field in a simple two-dimensional separation eddy, such as that found in the lee of a backward step or a bedform, for example. Figure 1 shows a schematic planform view of a lateral separation eddy; if this schematic is interpreted as a vertical slice of the flow field, it can equally well be considered a schematic for a simple two-dimensional eddy. A great deal is known about the details of flow in two-dimensional eddies (see, for example, the excellent review by Simpson [1989]), especially with regard to the spectral and spatial structure of vortices generated in the region of high shear and vorticity bounding the eddy, as described by Tani [1958], Mueller and Robertson [1963], Bradshaw and Wong [1972], and Etheridge and Kemp [1978], among others. Observations show approximately periodic shedding of vortices from the separation point, with subsequent growth and eventual dissipation of those vortices as they move downstream along the reattachment streamline. The period of vortex shedding is typically given by a Strouhal number (=fD/U) of about 0.2, where f is the shedding frequency, D is a separation length scale (the height or width of the obstacle behind which separation occurs, see Figure 1), and U is the mean velocity upstream of the separation point [Schlichting, 1979].

In the case of a truly two-dimensional eddy, vortices are generated with their axes perpendicular to the plane of the eddy and, as there is no mean shear in that direction by definition, the mean flow plays no role in altering the orientation of those vortices. Furthermore, there is no mean flow across the reattachment streamline (again, by definition in this two-dimensional flow); all exchange between the eddy and the main flow occurs through the fluctuating part of the flow field. Vortices act to enhance exchange across the reattachment streamline primarily through their role in the production of turbulence in this region.

In spite of the appeal of considering the flow field of a lateral separation eddy by analogy with that in a simple, two-dimensional eddy, there is a substantial flaw in the analogy. In the case of a lateral separation eddy, there is mean shear along the axes of vorticity shed from the separation point. This shear is associated with the structure of typical boundary layers; velocity is zero at the bed and increases rapidly and then more slowly with increasing distance from the bed. Considering a vortex shed from the separa-

tion point in Fig. 1 with a vertical axis (i.e., perpendicular to the page), it is clear both from simple reasoning and the conservation of vorticity equation that the vertical shear in the mean flow must produce tilting of the initially vertical vorticity into the streamwise direction (e.g., Holton, 1979, p. 92-94). This tilting produces a component of mean flow into the eddy near the bed and out of the eddy near the surface. Thus, in the lateral separation eddy case, the reattachment streamline is only a streamline in some vertically averaged sense; flow near the bed will be directed obliquely across that streamline into the eddy and flow near the surface will be directed obliquely across that streamline out of the eddy.

Given that bedload travels only very near the bed and that suspended load often has much greater concentrations near the bed than near the surface, the potential role of the secondary flow created by the vortex interaction with the riverine boundary layer is clear. Typically, this flow will advect relatively sediment laden water directly into the eddy at depth while evacuating relatively sediment-free water from the near-surface region. The result is direct advective transport of sediment into lateral separation eddies, not merely diffusive exchange across the reattachment streamline due to turbulence. Thus, lateral separation eddies have an advantage in trapping efficiency relative to purely two-dimensional eddies. One of the major points of this paper is that incorporating this effect in computational models is critical to accurate prediction of the morphology and temporal evolution of eddy deposits.

Experimental Evidence

To provide experimental evidence for the mechanism described above, several simple experiments in laboratory eddies were carried out. The first of these experiments involved measuring detailed time series of both downstream and cross-stream flow velocity within a lateral separation eddy with a flat, immobile bed using a laser-Doppler velocimeter (LDV). Detailed description of the flume employed and the LDV can be found in Nelson et al. [1993]. Referring to Fig. 1, the eddy geometry used in this first experiment incorporated an upstream channel width of 0.35m, a downstream channel width of 0.7m, and a flow depth of 0.07m. The mean downstream velocity in the upstream channel was about 0.31 m/s and the bed was bare plexiglass. In Fig. 2, two time series of cross-stream velocity measured during this experiment are

shown. Each of the two time series was measured at the same horizontal location along the reattachment streamline about 0.25m directly downstream from the point of separation; the time series in Fig. 2a was measured near the water surface, while that in Fig. 2b was measured very near the bed.

The most striking feature of these two time series is the obvious near-periodic pulsing associated with the passage of vortices shed from the separation point with a period of about 5s. The period of vortex shedding observed is in good agreement with that computed from the Strouhal number criterion, which yields a period of about 5.7s. For the observed values of streamwise velocity, the amplitude of the perturbations in cross-stream velocity shown in Fig. 2 produce instantaneous angular deviations between the mean streamline and the instantaneous flow direction of up to 90°.

The temporal mean velocity for the two time series in Fig. 2 is shown on the abscissa of each plot. For the near-surface flow, the average cross-stream velocity is negative, indicating that the mean flow at the surface is directed out of the eddy and toward the main channel. The temporal mean of the near-bed measurement, on the other hand, is positive, indicating that there is a secondary flow along the reattachment streamline driving flow into the eddy near the bed and out of the eddy at the water surface. Although this effect may seem minor, it is important to note that, for the observed values of streamwise velocity, the mean angular deviations between near-surface and near-bed measurements is approximately 30°. This angular deviation is comparable to those responsible for the initiation of point bars in curved channels [Rozovskii, 1957; Hooke, 1974; Nelson and Smith, 1989]. Thus, these observations, which are typical of all time series of cross-stream velocity along the upstream part of the reattachment streamline, strongly support the hypothesized secondary-flow-driven sediment trapping mechanism.

In addition to the mean secondary flow which acts to move sediment into the eddy, inspection of Fig. 2 suggests that even weak correlation between the vortex passage and suspended sediment concentration will also augment the movement of sediment into the lateral separation eddy. If there is a significant lateral concentration gradient between the main channel and the eddy, as is often the case, instantaneous flows from the main channel toward the eddy will tend to have higher concentrations of suspended

sediment than flows out of the eddy. Thus, because of temporal correlation between the sediment concentration and the velocity, the inward and outward variations in flow produced by the vortices will tend to produce transport of sediment into the eddy over and above that associated with the mean secondary flow. Note that this effect should only occur when there is sediment moving in suspension and the concentration in the main stem is greater than in the eddy. In situations where the main stem is severely sediment starved and concentration is higher in the eddy than in the main channel, it is plausible that this mechanism acts to remove sediment from lateral separation eddies.

Although the use of LDV is ideal for obtaining detailed time series information at individual points, it is time-consuming to use the technique to map out complex flow fields over a large spatial domain. In order to gain more complete spatial resolution of the development and decay of secondary flow along the reattachment streamline, a second experiment using particle tracking and video data acquisition was carried out. In this experiment, a lateral separation eddy was created by placing a 0.10-m-wide plexiglass block adjacent to the wall of an otherwise straight-walled, flat-bedded plexiglass flume. The flume used in this experiment was 0.40m wide, so the block created a separation eddy occupying roughly one quarter of the channel width. The flow depth for this experiment was 0.065m and mean streamwise velocity was about 0.10 m/s. The velocity field was digitized computationally from video records of neutrally buoyant pliolite particles illuminated using a 3-mm-thick sheet of laser light. By placing the laser sheet parallel with the bed, it was possible to track the motion of the pliolite particles moving in the flow and, by doing so, to determine entire two-dimensional fields of downstream and cross-stream velocity. By placing the laser sheet at different elevations above the bed, several such two-dimensional flow fields could be determined, and the vertical structure of the flow could be resolved.

In Fig. 3a, typical raw velocity vectors obtained from tracking pliolite particles over about 0.1s of video (four frames) are shown. This plot was created by overlaying tracks from several different periods of time, so that the temporal average, rather than the instantaneous field, could be evaluated. These sets of particle tracks can be spatially averaged to provide a uniform grid of mean velocity vectors. In Fig. 3b and

3c, examples of spatially and temporally averaged horizontal velocities fields determined 15 mm from the surface and 5mm from the bed, respectively, are shown. Looking along the line defined by $y=125$, the comparison of the near-bed and near-surface vectors clearly shows significant angular variation, with the near-bed vectors oriented into the eddy relative to the surface vectors. The turning of the near-bed velocity in Fig. 3c relative to Fig. 3b results from the secondary flow mechanics described above. As in the simple channel expansion, average angular deviations between the near-bed and near-surface flow along the reattachment streamline are on the order of 30° to 45°, although they are even higher at some locations. Considering the analogy with the role of secondary flow in the development of point bars in curved channels, it is easy to see that this mechanism must play a strong role in the development of bars in lateral separation zones, and that any physically realistic model of the process must incorporate this mechanism. Interestingly, it appears that this mechanism is also important in flow and bed evolution near channel diversion structures, as shown experimentally and computationally by recent research [Neary and Odgaard, 1993; Neary et al., 1994].

The creation of secondary flow through conservation of vorticity is clearly linked to the production of upwelling in the eddy itself. In Fig. 4a, contours of vertical vorticity show the position of the reattachment streamline as a region of strong counterclockwise vorticity. As noted above, the interaction of this vertical vorticity with the boundary layer shear in the mean flow will tend to produce streamwise vorticity. In Fig. 4b, continuity has been used with the spatial plots of streamwise and downstream velocity in order to compute the vertical gradient of vertical velocity near the bed. As the vertical velocity is zero at the bed, a positive value of the vertical gradient of vertical velocity corresponds to upward vertical velocity. As shown in Fig. 4b, $\frac{\partial w}{\partial z}$ tends to be positive on the eddyward side of the region of high vorticity and negative on the main channel side, corresponding to upwelling in the eddy and downwelling in the main channel. This provides strong support for the mechanism described above, and indicates the necessity of including the effect of secondary flow in a physically based model for deposition in eddies.

Development of the Numerical Model

If s, n, and z are taken as the streamwise, cross-stream, and vertical coordinates, respectively, the equations governing steady hydrostatic flow in a channel-fitted curvilinear coordinate system are given by the following:

$$\frac{1}{1-N}\frac{\partial u}{\partial s} - \frac{v}{(1-N)R} + \frac{\partial v}{\partial n} + \frac{\partial w}{\partial z} = 0 \tag{1a}$$

$$\frac{u}{1-N}\frac{\partial u}{\partial s} + v\frac{\partial u}{\partial n} + w\frac{\partial u}{\partial z} - \frac{uv}{(1-N)R} = \tag{1b}$$

$$\frac{-g}{1-N}\frac{\partial E}{\partial s} + \frac{1}{\rho}\left[\frac{1}{1-N}\frac{\partial \tau_{ss}}{\partial s} + \frac{\partial \tau_{ns}}{\partial n} + \frac{\partial \tau_{zs}}{\partial z} - 2\frac{\tau_{ns}}{(1-N)R}\right]$$

$$\frac{u}{1-N}\frac{\partial v}{\partial s} + v\frac{\partial v}{\partial n} + w\frac{\partial v}{\partial z} + \frac{u^2}{(1-N)R} = \tag{1c}$$

$$-g\frac{\partial E}{\partial n} + \frac{1}{\rho}\left[\frac{1}{1-N}\frac{\partial \tau_{ns}}{\partial s} + \frac{\partial \tau_{nn}}{\partial n} + \frac{\partial \tau_{zn}}{\partial z} + \frac{\tau_{ss} - \tau_{nn}}{(1-N)R}\right]$$

$$0 = -\frac{1}{\rho}\frac{\partial p}{\partial z} - g \tag{1d}$$

where u, v, and w are the velocities in the downstream, cross-stream, and vertical directions, respectively, E is the surface elevation, and R is the radius of curvature of the channel centerline. The quantity $1-N=1-n/R$ is the downstream metric associated with the curvilinear coordinate system, which is described formally by Smith and McLean [1984].

In the above equations, τ_{ss}, τ_{ns}, τ_{zs}, τ_{nn}, τ_{zn}, and τ_{zz} are the independent components of the deviatoric stress tensor. Viscous stresses in natural channels are typically negligible in comparison to Reynolds stresses and can be ignored. Rivers and streams are typically well-developed turbulent boundary layers with large horizontal length scales relative to their depth; therefore, these equations can be closed with a

scalar kinematic eddy viscosity that emphasizes vertical diffusion of momentum. If this assumption is made, the Reynolds stresses may be expressed in terms of the rate of strain tensor. In the given coordinate system, this relationship results in the following equations for the stress components:

$$\tau_{ss} = 2\rho K\left(\frac{1}{1-N}\frac{\partial u}{\partial s} - \frac{v}{(1-N)R}\right) \quad \tau_{nn} = 2\rho K\left(\frac{\partial v}{\partial n}\right) \quad \tau_{zs} = \rho K\left(\frac{1}{1-N}\frac{\partial w}{\partial s} + \frac{\partial u}{\partial z}\right) \tag{2}$$

$$\tau_{zz} = 2\rho K\left(\frac{\partial w}{\partial z}\right) \quad \tau_{zn} = \rho K\left(\frac{\partial w}{\partial n} + \frac{\partial v}{\partial z}\right) \quad \tau_{ns} = \rho K\left(\frac{1}{1-N}\frac{\partial v}{\partial s} + \frac{u}{(1-N)R} + \frac{\partial u}{\partial n}\right)$$

Equations 1 and 2 are the basic statements of conservation of mass and momentum for the flow problem to be addressed here. While numerical solution of these full equations is certainly possible, the solutions are strongly dependent on the specification of the eddy viscosity. In simple flows, similarity or dimensional constraints can be used to develop relatively robust characterizations of this quantity, but in complex flows, the presence of a variety of length scales make this much more difficult, if not impossible. In engineering fluid mechanics, the most common approach to this difficulty is the use of semi-empirical turbulence-transport models [Rodi, 1980], which specify the eddy viscosity field by advecting and dissipating surrogates for the turbulence velocity and/ or length scales. Even these relatively general closure techniques require adjustment of empirical constants in order to yield reasonable results and, despite their relative complexity, are not particularly good for treating flows with separation zones. In view of this difficulty and the demands on computational resources required for the solution of equations 1 and 2, we elect to use a simpler approach that separates the problem into a 2-dimensional flow routing problem weakly coupled to a solution for vertical structure. While this approach is clearly approximate, the improvements obtained using a much more complex treatment may be small relative to the overall uncertainty stemming from inexact specification of the turbulence field. This is particularly true for the problem that is considered herein, which is a flow over complex topography that, although predominantly boundary layer-like in nature, includes components of both free-shear layers and wakes.

Vertically averaged flow

Solving the 2-dimensional routing part of this flow problem requires development and solution of the vertically averaged flow equations. Vertically averaging the mass and momentum conservation equations and writing the velocity components as a sum of their vertical average and the deviation from that average (e.g., $u(z) = \langle u \rangle + u'(z)$) yields:

$$\frac{1}{1-N}\frac{\partial}{\partial s}(\langle u\rangle h) - \frac{\langle v\rangle h}{(1-N)R} + \frac{\partial}{\partial n}(\langle v\rangle h) = 0 \tag{3a}$$

$$\frac{1}{1-N}\frac{\partial}{\partial s}(\langle u\rangle^2 h) + \frac{\partial}{\partial n}(\langle u\rangle\langle v\rangle h) \frac{2\langle u\rangle\langle v\rangle h}{(1-N)R} + F' = \frac{-gh}{1-N}\frac{\partial E}{\partial s} - \frac{(\tau_{zs})_B}{\rho} + \tag{3b}$$

$$\frac{1}{\rho}\left[\frac{1}{1-N}\frac{\partial}{\partial s}(\langle \tau_{ss}\rangle h) + \frac{\partial}{\partial n}(\langle \tau_{ns}\rangle h) - 2\frac{\langle \tau_{ns}\rangle h}{(1-N)R} + \frac{1}{1-N}(\tau_{ss})_B\frac{\partial B}{\partial s} + (\tau_{ns})_B\frac{\partial B}{\partial n}\right]$$

$$\frac{1}{1-N}\frac{\partial}{\partial s}(\langle u\rangle\langle v\rangle h) + \frac{\partial}{\partial n}(\langle v\rangle^2 h) + \frac{(\langle u\rangle^2 - \langle v\rangle^2)h}{(1-N)R} + G' = -gh\frac{\partial E}{\partial n} - \frac{(\tau_{zn})_B}{\rho} + \tag{3c}$$

$$\frac{1}{\rho}\left[\frac{1}{1-N}\frac{\partial}{\partial s}(\langle \tau_{ns}\rangle h) + \frac{\partial}{\partial n}(\langle \tau_{nn}\rangle h) + \frac{\langle \tau_{ss} - \tau_{nn}\rangle h}{(1-N)R} + \frac{1}{1-N}(\tau_{ns})_B\frac{\partial B}{\partial s} + (\tau_{nn})_B\frac{\partial B}{\partial n}\right]$$

where

$$F' = \frac{1}{1-N}\frac{\partial}{\partial s}(\langle u'^2\rangle h) + \frac{\partial}{\partial n}(\langle u'v'\rangle h) - \frac{2\langle u'v'\rangle h}{(1-N)R} \tag{3d}$$

$$G' = \frac{1}{1-N}\frac{\partial}{\partial s}(\langle u'v'\rangle h) + \frac{\partial}{\partial n}(\langle v'^2\rangle h) + \frac{(\langle u'^2\rangle - \langle v'^2\rangle)h}{(1-N)R}$$

In these equations, $\langle\ \rangle$ indicates vertical averaging, while primes indicate deviations from the vertical average of the primed variable, as noted above. The surface elevation is given by $z=E(s,n)$, the bed elevation is given by $z=B(s,n)$, and the subscript B indicates that the subscripted variable is evaluated at the bed. The terms F' and G' are vertically averaged momentum fluxes that arise because the vertical profiles

of the streamwise and cross-stream velocities are not constant; they have a strongly varying vertical distribution. As a result, momentum fluxes computed assuming that $\langle u^2 \rangle = \langle u \rangle^2$, $\langle v^2 \rangle = \langle v \rangle^2$, and $\langle uv \rangle = \langle u \rangle \langle v \rangle$ will be in error. In general, these terms are relatively small and the error incurred by neglecting them is slight, but in the absence of strong topographically or curvature driven convective accelerations, these terms may be responsible for important physical effects, as shown, for example, by Shimizu et al. [1989]. In the model described herein, these terms are only included in an iterative sense, as described briefly below in the discussion of the vertical structure of the flow.

In order to close Eq. 3a-c, all stress terms must be expressed in terms of the vertically averaged velocities. For the bottom stress terms, this is accomplished by assuming that all bed stresses associated with the interaction of normal and lateral stresses with the sloping bottom (the last two terms in both Eq. 3b and 3c) are negligible relative to bottom stresses associated with vertical shears, which are expressed using a simple drag closure as follows:

$$\frac{(\tau_{zs})_B}{\rho} = C_d[\langle u \rangle^2 + \langle v \rangle]^{1/2} \langle u \rangle \tag{4a}$$

and

$$\frac{(\tau_{zn})_B}{\rho} = C_d[\langle u \rangle^2 + \langle v \rangle]^{1/2} \langle v \rangle \tag{4b}$$

The other vertically averaged Reynolds stress terms in Eq. 3b and 3c are modeled using the vertical average of the expressions in Eq. 2 assuming that the eddy viscosity can be replaced by its vertically averaged value. The only exception to this is that, near steep banks or vertical flume walls, the form of drag closure shown in Eq. 4 is also used for lateral stresses. Using the vertically averaged eddy viscosity neglects effects associated with the fact that the eddy viscosity may be correlated with the velocity structure in the vertical. Although these effects may be treated by inclusion of appropriate additional vertical correlation terms in F′ and G′, it is questionable whether the additional complexity is warranted by the simple turbulence

closure employed here. We choose to neglect these terms; including them may be correct in a mathematical sense, but it is unlikely that the results would be improved in any physically meaningful manner.

Using the closures described above, the system of equations 3a-d is solved computationally on a curvilinear orthogonal grid using relatively standard techniques. First, the streamwise and cross-stream momentum equations are solved explicitly for the vertically averaged velocity subject to known (guessed) surface elevation and velocity fields; the initial guess is taken from a simple steady one-dimensional flow solution. The explicit technique incorporates upwind differencing and operator splitting [Press et al., 1986], which considerably enhance stability and convergence characteristics. Second, the surface elevation is calculated implicitly using the Simple method [Patankar, 1980], which comprises an alternating-direction implicit scheme with operator splitting and a tridiagonal matrix solver. Finally, the elevation and velocity fields are updated using relaxation, and the process is repeated until mass and momentum conservation is satisfied to a very high degree of accuracy. The use of relaxation rather than a time-stepping model greatly shortens the required computation time, especially if care is taken in selecting different relaxation coefficients for elevation and velocity. In general, the best convergence for separating flows was found with relaxation coefficients of around 0.6 for elevation and 0.3 for velocity. For simple unseparated flows, over-relaxation (i.e., relaxation coefficients greater than one) can be used to good advantage. The techniques employed are chosen to minimize numerical diffusion to the greatest degree possible with a simple approach. Boundary conditions require specification of surface elevation at the downstream end of the computational reach and vertically averaged velocities at the upstream end of the computational reach. Alternatively, a critical Froude number criterion may be specified at either end of the reach; although this is usually not a common boundary condition, it is ideal for computations immediately upstream or downstream of rapids.

The numerical solution of Eqs. 3a-d yields the vertically averaged downstream and cross-stream velocities, the bottom stress vector, and the surface elevation field. To compute the vertical structure and the secondary flows, the turbulence model must be considered in more detail.

Vertical structure of the flow

Determination of the vertical structure of the flow is accomplished by prescribing a simple eddy viscosity structure and an associated similarity vertical structure along and across the streamlines of the vertically averaged flow given by the numerical solution of the vertically averaged flow equations. Specification of the eddy viscosity structure for a flow situation with boundary layer, mixing layer, and wake structure is not possible in general, but for the case of lateral separation zones in rivers, the flow is still principally characterized as a thin shear layer, as rivers are typically much shallower than they are wide or long, and the boundary layer length scales are dominant. This can be seen from comparison of the velocity and length scales making up the eddy viscosities for each of the basic components of the flow.

Eddy viscosity is generally defined in terms of a turbulent length scale multiplied by a turbulent velocity scale, $K = L_t U_t$. In a boundary layer in an open channel, the near-bed velocity scale is given by the shear velocity, u_*, defined as $[\tau_b/\rho]^{1/2}$. The near-bed length scale of turbulent exchange is given by von Karman 's coefficient (=.407,Long et al., 1993), multiplied by the distance from the bed. The linear dependence is found from the bed up to about 20% of the boundary layer thickness. Above this region, a number of relations have been proposed for the eddy viscosity, including parabolic, polynomial, exponential, and constant functional dependences. Using the Prandtl mixing length analogy, which assumes that the velocity scale may be written as the length scale multiplied by the local shear in the mean velocity field, and hence that the the eddy viscosity is given by $K = L_t^2 \frac{\partial U}{\partial z}$, where z is the coordinate in the direction of maximum shear, Patankar and Spalding [1970] found a best-fit length scale consisting of the linear profile described above up to about 20% of the boundary layer thickness matched to a constant length scale throughout the rest of the boundary layer. The vertical average of the length scale is on the order of 0.1 times the boundary layer thickness (equivalent to the depth for the case considered here), which reflects the role of limited vertical flow extent in controlling the length scale of turbulent exchange. In the case of either a wake or a mixing layer, the length scale of the turbulence is proportional to the width of the feature, and the velocity scale is proportional to the maximum velocity difference across the feature [Schlichting, 1979, p.

729-754]. Using the Prandtl mixing length analogy, the maximum velocity difference can be parameterized by the length scale multiplied by the local shear, so the eddy viscosity is given by $K = L_t^2 \frac{\partial U}{\partial y}$, where y is the coordinate perpendicular to the principal flow direction. For plane mixing layers and wakes, the best fit mixing lengths are given by about 70% of the mixing layer width and 10% of the wake width, respectively [e.g., Rodi, 1980, p. 17; Schlichting, 1979, p. 742]. These values are only accurate in the region of the flow where the mean flow is self-preserving (self-similar). For the mixing layer, this is true when $xU/\nu > 4 \times 10^5$, where x is distance downstream of the origin of the mixing layer, U is the free stream velocity outside the mixing layer, and ν is the kinematic velocity [Tennekes and Lumley, 1972, p.128]. For the wake, this is true about 50-80 obstacle diameters downstream of the separation point [Bradshaw and Wong, 1972; Tennekes and Lumley, 1972, p. 115].

For the case of a quasi-two-dimensional shear layer located in a relatively shallow open channel flow with bed and surface roughly parallel to the plane of quasi-two-dimensionality, there is a strong constraint placed on the development of turbulent length scales within the shear layer because of the essential three-dimensional nature of turbulence. The structure of the flow along the upstream part of the reattachment streamline of a lateral separation eddy can be expected to look substantially like a mixing layer. However, comparison of the length scales of the mixing layer and the boundary layer in which it is located indicates that the mixing layer length scale will be comparable to that of the boundary layer when the width of the mixing layer is a small fraction (1/7) of the depth. As the mixing layer develops downstream of this point one must expect that the same poorly understood processes that limit the growth of the boundary layer length scales must begin to alter the length scales in the mixing layer. Although this is only a rough scaling, it seems reasonable to conclude that the length scales of the turbulence will not continue to increase in response to the growth of the mixing layer, but will instead be limited to a value comparable to that found in a normal boundary layer. Similarly, well downstream of the separation zone where one might expect the presence of wake-like turbulence, wake length scales are far too large to be present in the boundary layer, at least in the sense of three-dimensional turbulence structures. Thus, it seems reasonable to assume that,

except for the region very near the separation point, the length scales characterizing an isotropic eddy viscosity should be the boundary layer length scales.

It is important to note that the dominance of boundary layer length scales in the turbulence field does not preclude the possibility that there is large-scale variability associated with the free shear layers present in the flow, it only means that these larger structures are principally two-dimensional, and should not be treated as turbulence without care. Although, the presence of large-scale unsteadiness in two-dimensional separated flows is well known [e.g.,Simpson, 1989], parameterization of their effects in principally boundary-layer-like flows is difficult. The use of a large-eddy simulation or discrete vortex model avoids this parameterization problem at the cost of greatly increased use of computational resources. As the intent here is to use the flow model in an iterative sense to predict bed evolution, the penalty associated with using a much more complex flow model is multiplied many times over, resulting in unacceptably slow computational predictions. Thus, for this problem, it is necessary to prescribe a simple technique to parameterize these effects at least in a crude manner.

Using the mixing length analogy, the assumption that the turbulence is dominated by the boundary layer length scales is equivalent to assuming that the boundary layer eddy viscosity can be used without modification over most of the flow, since lateral shears are generally much smaller than vertical ones. The only exception is very near the separation point, where lateral shears can be comparable to vertical ones, in regions where a lateral shear is present but the velocity is near zero so there is little vertical shear (e.g., at the center of an eddy), and near steep banks. As noted above, near steep banks or vertical walls a drag coefficient closure is employed, so this situation is not problematic. To deal with the other two situations and to incorporate the effects of quasi-two-dimensional unsteadiness along the reattachment streamline, we modify the vertically averaged eddy viscosity in a simple manner consistent with the classical free shear layer expressions. There are essentially two parts to the approach used here. First, we assume that the vertical exchange of momentum can be described by a typical open channel eddy viscosity and second, we modify the vertically averaged eddy viscosity to include the effect of flow separation.

For the vertical exchange of momentum by turbulence in boundary layer flows with lateral flow separation, we use the same eddy viscosity we use in flow problems without flow separation. Specifically, we use the eddy viscosity given by Rattray and Mitsuda [1974]:

$$K_v = ku_*z(1 - z/h) \qquad z \leq 0.2h \tag{5}$$

$$K_v = ku_*h/\beta_1 \qquad z > 0.2h$$

where h is the flow depth, u_* is the local shear velocity, k is von Karman 's coefficient and $\beta_1 = 6.24$. This eddy viscosity is consistent with the length scale of Patankar and Spalding [1970], is a good analytical approximation to the best-fit numerical profile employed by Smith and McLean [1977], and it provides an excellent fit to the pipe flow data analyzed by Long et al. [1993]. The vertical average of this eddy viscosity is given by $<K_v> = ku_*h/\beta_2$, where $\beta_2 = 6.87$. To treat lateral separation problems, we assume that the eddy viscosity used in the solution of the vertically averaged equations of motion be specified by adding a correction factor to the vertical average of the Rattray-Mitsuda eddy viscosity given above. The correction factor is set by considering the best-fit mixing layer and wake eddy viscosities, which are given by $K_{ml} = 0.014 b_{0.1} U$ and $K_w = 0.022 C_d d U$ respectively, where $b_{0.1}$ is the lateral distance between the points where the velocity is 10% and 90% of the free stream velocity outside the mixing layer, U is the free stream velocity, C_d is the wake drag coefficient, and d is the diameter of the obstacle producing the wake [Schlichting, 1979, p. 738, p. 743]. Note that the eddy viscosity increases downstream as the mixing layer spreads, but is constant in the wake far field. As noted above, we expect that the length scales in these expressions will be modified by the presence of the bed and surface in the case of relatively thin lateral separation eddies, as studied here. Considering this limitation in both the mixing layer and wake eddy viscosity expressions, a general eddy viscosity can be expressed as AUh, where h is the average flow depth, U is the free-stream velocity, and A is a constant. Considering that the mixing layer length scale is equivalent to the boundary layer one when the width of the mixing layer is $O(10^{-1})$ times the depth leads to the conclusion that the constant A is of order 10^{-3}. However, this neglects effects associated with quasi-

two-dimensional unsteadiness, which may produce effective length scales similar to the flow depth, resulting in a value of A of order 10^{-2}. We expect the value of A to fall somewhere between these two extremes. Thus, the eddy viscosity used in the vertically averaged flow solution is taken as follows:

$$K = \langle K_v \rangle + AUh \tag{6}$$

where U, the free-stream velocity, is computed as the cross-sectional average of the flow velocity upstream of the separation point and h is the average flow depth.

Noting that U/u_* is O(10) in the flows of interest, the range of A (10^{-3} to 10^{-2}) results in a correction to the vertically averaged boundary layer eddy viscosity of between 10% and 100%. Even using the maximum value, the correction is a relatively modest one compared to adjustments in cross-stream diffusivities used in other computational models, which often use horizontal diffusivities an order of magnitude larger than the vertical ones. This may be partially due to the need for artificially high horizontal diffusivities to ensure numerical stability of the solution, but it is often a result of parameterization of advective processes, such as those associated with shear dispersion and effects of secondary flows, in a diffusive manner. As the intent here is to maintain resolution of the operative advective processes to the greatest degree possible in a simple modeling approach, this is not acceptable. Although the approximate approach described here requires setting the value of A (within the reasonable limits described above), the formulation is based on the fundamental processes, albeit in a crude manner using scaling arguments. The choice used for the value of A is resolved experimentally, as discussed below.

Using the argument developed by Nelson and Smith [1989a] for the quasi-linearity of the shear stress profile even in complex boundary layer flows, and using the vertically averaged flow solution and the vertical eddy viscosity distribution, it is possible to define the vertical structure of the flow along the streamlines of the vertically averaged flow as follows:

$$u_s(z) = (u_*)_s \int_{\varsigma}^{\varsigma} \frac{1-\varsigma}{\kappa} d\varsigma = (u_*)_s f(\varsigma,\varsigma_0) \tag{7}$$

where the subscript s indicates that the variable is evaluated along the streamlines of the vertically averaged flow, κ is defined as $K/u_{*_s}h$, $\varsigma = z/h$, and $\varsigma_0 = z_0/h$, where z_0 is the roughness length. In addition, u_{*_s} is defined as follows:

$$u_{*_s} = \left[\frac{(\tau_{zs})_B^2 + (\tau_{zn})_B^{2}}{\rho} \right]^{1/2} \tag{8}$$

where $(\tau_{zs})_B$ and $(\tau_{zn})_B$ are defined in the vertically averaged flow solution through Eq. 4. Using these relations, it is also possible to define the relation between the drag coefficient and the vertical structure:

$$C_d = \left[\int_{\varsigma}^{1} f(\varsigma,\varsigma_0) d\varsigma \right]^{-2} \tag{9}$$

The solution of the vertically averaged flow solution along with Eqs. 7-9 yields an approximation of the full three-dimensional flow field including velocity, shear stress, and surface elevation. This solution consists of a flow directed along the streamlines of the vertically averaged flow field with a simple similarity vertical structure. To treat flows across those streamlines that produce no net flux across the streamlines (secondary flows), the approach used for determination of secondary flows in channel bends is generalized using the scaling presented by Nelson and Smith [1989a,b]. Provided that the vertical structure of the primary flow had relatively weak shear away from the boundary (as is the case in most riverine flows), they showed that curvature-driven secondary flows could be computed from a simple momentum balance between vertical stress divergence, the pressure gradient, and the convective accelerations computed from the vertically averaged flow and the similarity velocity structure. Using this simple balance along with the assumption of a no-slip condition at the bed and no surface stress, the curvature-driven secondary flow acting transverse to the streamlines of the vertically averaged flow (denoted u_{trans} and defined as positive

toward the center of curvature) is given by

$$u_{trans} = \frac{(u_*)_s\, h}{R_s}\left[C_d^{1/2}\, Gf(\zeta,\zeta_0) - g(\zeta,\zeta_0)\right] \tag{10}$$

where

$$g(\zeta,\zeta_0) = \int_{\zeta 0}^{\zeta} \frac{1}{\kappa} \int_{\zeta'}^{1} f^2(\zeta,\zeta_0)\, d\zeta\, d\zeta' \tag{11}$$

and

$$G = \int_{\zeta 0}^{1} g(\zeta,\zeta_0)\, d\zeta \tag{12}$$

and where R_s is the local radius of curvature of the vertically averaged streamlines. Similarly, the local perturbation stress field associated with the curvature-driven secondary flow is given by

$$\tau_{trans}(\zeta,\zeta_0) = \frac{\rho\,(u_*)_s^{\,2}\, h}{R_s}\left[C_d^{1/2}\, G\,(1-\zeta) - \int_{\zeta}^{1} f^2(\zeta,\zeta_0)\, d\zeta\right] . \tag{13}$$

where the stress acts on a horizontal plane (i.e., a plane with a vertical normal) in a direction transverse to the vertically averaged streamline.

Using Eqs. 10-13, curvature-driven velocities and stresses can be computed from the results of the vertically averaged flow solution and an assumed form of the vertical eddy viscosity. These are added in a vector sense to the stress and velocity fields developed using the vertically averaged flow solution and the along-streamline vertical structure in order to generate a complete approximation to flow in channels with lateral flow separation. Notably, the bed stresses associated with the secondary flows produce turning of the total bottom stress vector toward the center of curvature relative to the vertically averaged streamlines of the flow. As will be demonstrated below, this turning plays an important role in lateral separation zone

sedimentation.

Sediment-transport model

To predict the evolution of bed topography in response to the flow field in the vicinity of a lateral separation zones, relations between flow variables and fluxes of sediment are combined with an integral statement of the conservation of sediment mass. Transport of sediment as bedload is treated separately from transport of sediment in suspension. The results for bedload cases presented in this paper are based on the bedload equation presented by Yalin (1963) in conjunction with a simple algorithm for including the effect of bed slope on the sediment fluxes. If τ_{SF} is the magnitude of the vector skin friction boundary shear stress on the bed, then the sediment flux in the vector direction of the stress is given by the Yalin equation as

$$Q_{tot} = 0.635\left(\frac{\tau_{SF}}{\rho}\right)^{1/2} DS\left[1 - \frac{1}{\gamma S}\ln(1 + \gamma S)\right] \qquad (14)$$

where D is the particle diameter, S is the local excess shear stress defined by $(\tau_{SF} - \tau_c)/\tau_c$, and $\gamma = 2.45 (\rho/\rho_s)^{0.4} (\tau_c/(\rho_s-\rho)gD)^{0.5}$. The variables ρ and ρ_s are the density of the fluid and the sediment, respectively, and are taken to be 1000 kg/m^3 and 2650 kg/m^3 .

If the actual bottom stress values predicted by the flow model is inserted in equation (14), the calculated sediment fluxes will not include the modification of those fluxes by gravitational forces, since the bedload equation does not take the effect of bed slope into account. The slope effect is expected to be relatively large in cases where the boundary shear stress is only slightly larger than the critical shear stress for the initiation of particle motion (i.e., low transport stages). This is due to the fact that, at these low transport stages, sediment particles tend to roll, rather than saltate, and therefore remain in contact with the bed most of the time (Wiberg and Smith, 1985). Conversely, we expect the gravitational correction to be relatively small in the case of saltation (higher transport stages), wherein the direction of travel of the moving particle is almost entirely determined by the direction of flow. While the actual numerical error

incurred by neglecting the effect of bed slope may be negligible compared to the total sediment flux, the small variation in the direction of the sediment flux vector on the bed can be important in the calculation of stable channel morphology, especially in the case of low transport stages. To treat this part of the sediment-transport problem, we use the gravitational correction algorithm proposed by Hasegawa [1984]. In its original form, this equation is used to predict the correction to cross-stream sediment fluxes in a flow where the boundary shear stress is directed principally downstream (with a small correction for secondary flows), which is not a reasonable approach for the problem considered here. Thus, the approach is generalized to predict gravitational corrections to the bedload flux as a result of slopes in the direction orthogonal to the bottom stress vector. Using this generalization, the gravitational correction can be expressed as follows:

$$Q_g = Q_{tot}\left[\frac{1}{\mu_s \mu}\left(\frac{\tau_c}{\tau_b}\right)^{1/2}\frac{\partial B}{\partial \alpha}\right] \tag{15}$$

where τ_b refers to the vector boundary shear stress (including the effects of secondary flow), μ_s is a static coefficient of friction (≈ 1.0), μ is a dynamic coefficient of friction (≈ 0.43)and α is a coordinate transverse to the boundary shear stress vector. Note that this method explicitly excludes corrections to sediment fluxes resulting from bed slope in the direction of the bottom stress vector, unlike the pseudo-stress gravitational correction method presented by Nelson and Smith [1989b].

After using the computed stress field to find Q_{tot}, the gravitational correction is computed and the resulting sediment flux vector is separated into its components (Q_s and Q_n) in the orthogonal curvilinear coordinate system described above.

In that coordinate system, the equation relating bedload sediment fluxes on the bed to the rate of erosion and deposition is given by

$$\frac{\partial B}{\partial t} = -\frac{1}{c_B}\left[\nabla\cdot\vec{Q}\right] = -\frac{1}{c_B}\left[\frac{1}{1-N}\frac{\partial Q_s}{\partial s} + \frac{\partial Q_n}{\partial n} - \frac{Q_n}{(1-N)R}\right] \tag{16}$$

where B denotes the elevation of the bed with respect to an arbitrary datum and where c_B is the concentration of sediment in the bed ($c_b \approx 0.65$).Assuming that the flow and sediment transport can be treated in a quasi-steady manner, and using Eq. 16 to compute erosion and deposition rates, it is possible to compute the bed evolution by iteratively solving for the flow and the sediment transport with a suitable small time step, as described by Nelson and Smith (1989a,b).

Treatment of sediment moving in suspension can be accomplished in a variety of ways depending on the characteristics of the flow and the sediment grain sizes. If the time required for sediment particles to settle to the bottom is short relative to the time required for particles to be advected over spatial scales associated with significant changes in bottom stress, and if lateral diffusion is negligible, total load equations, such as that proposed by Engelund and Hansen [1967],can be used. If these conditions are not met, a solution of the advection-diffusion equation expressing mass conservation for the suspended sediment is required. Unfortunately, although numerical solutions of this three-dimensional equation have been developed, solutions in geometrically complex domains are computationally time-consuming. As the flow model used here uses a simple closure for turbulence and an approximate treatment for computing vertical structure, solution of the full three-dimensional advection-diffusion equation is of questionable value, because errors in the predicted diffusivities and flow field will overwhelm any advantage of a three-dimensional treatment of the suspended sediment. To proceed in a consistent manner, the advection-diffusion treatment used herein is developed in parallel with the flow solution; the full equation is reduced to a vertically averaged equation describing the basic sediment routing and a separate approximate solution for the vertical structure [Nelson, Schmeeckle, and Bennett, in preparation]. The vertically averaged part of the problem, which focuses on treatment of advection and lateral diffusion of the sediment, explicitly incorporates the shape factors developed from the vertical structure part of the problem. Thus, the full problem can be reduced to a simple two-dimensional numerical solution along with a simple,

prescribed vertical structure. This is both computationally effective and consistent with the degree of approximation used in the flow solution.

Testing of the Numerical Model

Flow Field

To test the numerical model described above, results for both flow and bed evolution were computed for the laboratory situation described above and compared to flow and bed evolution measurements made in the laboratory. To determine the value of A in Equation (6), model results were obtained over the range of reasonable values discussed above and compared to streamwise flow measurements made across the mixing layer on the channelward side of a simple laboratory eddy, as shown in Fig. 5. This region was chosen for detailed comparison because the velocity structure in the shear layer is most sensitive to A. In general, solutions found over the entire range of values for A are reasonably close to the data, but there are some consistent discrepancies. The fit in the upstream channel is relatively poor; this results from the choice of an inlet velocity boundary condition that is uniform across the channel. Moving downstream, the growth of the lateral boundary layer near the flume wall is clear, and a longer upstream reach would clearly predict better results for the cross-stream structure in the narrow upstream channel at the expense of a larger computational grid. Comparing results for various values of A, it is clear that, although all the fits are reasonably good, a value in the middle of the range yields the best results. The solution in Fig. 5a, which uses a value of 0.001 for A, is essentially indistinguishable from solutions computed using smaller values or zero for A, reflecting the fact that for small values, the boundary layer eddy viscosity dominates the problem. However, as is clear from Fig. 5a, the model overpredicts the shear across the reattachment streamline if this value (or a smaller one) is employed for A. In addition, this choice of A yields an underprediction of the magnitude of the upstream velocity in the eddy close to the separation point and an overprediction of the magnitude of the return flow further from the obstacle, reflecting the fact that momentum diffusion is underpredicted along the free shear layer near the separation point. In contrast,

using a value for A of 0.02 produces the opposite problem, with too little shear across the shear layer and underprediction of the magnitude of the return flow farther from the obstacle. In Figs. 5b and 5c, where A is 0.005 and 0.01, respectively, the fits are significantly better, although not perfect. Generally, it appears that a value of 0.005 is the best, especially for comparisons farther from the separation point. At least with this data set, it is probably not appropriate to attempt to set this value any more closely, but the fact that the best-fit value clearly falls within the range determined by dimensional considerations and comparisons with classical free shear layer flows is encouraging. From this point on, the computations presented herein use a value of A of 0.005. This represents a relatively modest correction to the boundary layer eddy viscosity, resulting in lateral diffusivities typically less than a factor of two greater than vertical ones, except in regions where the bottom stress is very low or zero, such as near the center of the eddy, where the lateral diffusion term dominates Equation (6).

In Fig. 6, numerical predictions of vertically averaged velocity, vector shear velocity, and surface elevation are shown for the conditions of the rectilinear expansion laboratory experiment modified by the addition of a natural sand bed (well-sorted sand with $D_{50} = 0.9$mm) and a mean depth of 0.10m. These parameters reflect the initial flow conditions for the bed evolution experiment described below. Note that the plotted vectors in Figs. 6a and 6b are subsampled from the full computational grid, which is three times more dense than shown in these plots. The vertically averaged velocity field in Fig. 6a shows a typical recirculating flow pattern, with rapidly decelerating flow in the main channel, and reattachment at around 7 obstacle widths downstream of the separation point. This mean reattachment distance is in good agreement with that found by other researchers (Bradshaw and Wong, 1972; Etheridge and Kemp, 1978; Mueller and Robertson, 1963) and is in much better agreement with measured values than models using different approaches, which often predict reattachment lengths significantly shorter than observed [e.g., Ponce and Yabusaki, 1981; Yeh et al., 1988], presumably as a by-product of high numerical diffusion or exaggerated lateral diffusion coefficients required for stability. In this flat-bedded eddy, the maximum upstream velocity is found near the flume wall at about the midpoint of the eddy. While this is consistent

with the flow measurements in Fig. 5, it is somewhat different from the result found in a topographically complex natural eddy, as will be discussed below.

The boundary shear stress is typically much smaller in the eddy than in the main part of the channel, as it depends approximately on the velocity squared. Because of the difference in magnitude across the flow, plots of bottom stress that show detail within the eddy are difficult to make. To avoid this problem, we show a plot of vector shear velocity in Fig. 6b. The vector shear velocity has the same direction as the boundary shear stress, but its magnitude is the square root of the boundary shear stress over the density. As can be seen by comparison of Fig. 6a and Fig. 6b, the shear velocity is directed into the eddy relative to the vertically averaged velocity, reflecting the effect of secondary flows computed in the model, and in agreement with the observations discussed above. Note that, in the absence of secondary flow effects, the bottom stress and the vector shear velocity would have the same orientation as the vertically averaged velocity vectors shown in Fig. 6a. The tendency for the bottom stress to be directed toward the center of the channel at the upstream cross-section is associated with rapid deceleration of the flow near the flume walls as a result of the assumption of uniform inlet velocity and the growth of lateral boundary layers.

In Fig. 6c contours of surface elevation are shown over a longer reach than the vector plots in Figs. 6a and 6b in order to clarify the relaxation of the flow back to normal downstream flow conditions. In a streamwise sense, the surface elevation field consists of a steep drop in the narrow, high-velocity upstream channel with a minimum in elevation somewhat downstream of the separation point, followed by an increase in surface elevation driven by the strong deceleration in the flow. As the deceleration decreases downstream, the surface elevation reverts to a downstream slope, albeit with a much lower gradient in this low-velocity flow relative to the gradient in the upstream channel. In the eddy, there is a local minimum in surface elevation near the eddy midpoint and a local maximum near the reattachment point. Thus, the pressure field generated primarily through the response of the main channel flow to the channel widening results in an eddy surface elevation field that accelerates the flow upstream along the flume wall. This is the basic mechanism for the production of recirculation zones even in complex situations, but it is espe-

cially clear in this simple case.

In Figs. 7a and 7b, contours of downstream and cross-stream flow are shown for the cross-section at the center of Figs. 6a and 6b, which corresponds closely to the section for which upstream velocities in the eddy are greatest. The contours of streamwise velocity are not particularly interesting, showing typical flow structure with strong shear near the bed and much weaker shear in the flow interior. This is primarily because the vertically averaged flow is mostly in the streamwise direction at this section, so all secondary flows tend to be in the cross-stream flow direction. This is not generally the case, as we compute secondary flows transverse to the streamlines of the vertically averaged flow solution, rather than just in the cross-stream direction. In Fig. 7b, the contours of the cross-stream velocity show strong secondary flow effects, with a cell of flow directed into the eddy at depth in the main channel, and another much weaker cell directed toward the center of the eddy from the return flow channel near the flume wall in the eddy. Note that, although the strongest secondary flows are generated near the center of the channel, the greatest angular deviations between the vertically averaged velocity and the bottom stress are found near the reattachment streamline at a distance of about 0.1m from the channel centerline. This is a direct result of the fact that the streamline curvature becomes greater moving toward the eddy from the main channel.

Bed Evolution

To provide a data set to test the sediment transport and bed evolution aspects of the model presented herein, the laboratory experiment for a simple rectilinear channel expansion was repeated with a movable bed and the bed topography was measured at discrete intervals as it evolved. The bed was composed of 0.9mm sand, which traveled exclusively as bedload for the chosen flow conditions. The initial flow depth was 0.10m and the discharge was 22 l/s. The bed evolution was monitored over a two meter-long section immediately downstream of the separation point for a period of several hours, but the bed was close to the equilibrium condition after about two hours. Some very slow modification of the bed morphology continued after this period along with quasi-periodic temporal variation associated with the passage of

small bed forms in the main channel. To demonstrate the effect of secondary flows in altering the sediment flux and erosion/ deposition patterns, computational results were computed for the laboratory case with and without the secondary flow correction over the two hour period during which the majority of bed evolution took place. In Figs. 8a and 8b, the computed changes in the bed for the first twelve minutes of evolution are shown for the case with and without secondary flow effects, respectively. In both cases, the first substantial change to the initially flat bed is the deposition of a bar in the main channel downstream of the channel expansion. This is associated with the deceleration of the flow in this region. As a result of the lateral spreading of the flow, this bar tends to grow more rapidly on the eddyward side of the main channel. In Fig. 8a, the effect of secondary flow is seen as a linear ridge extending upstream from the eddyward side of the mid-channel bar. This feature is not present in Fig. 8b and, in general, the deposition on the eddyward side of the bar is lower throughout the first twelve minutes. As the bar develops and moves downstream, a local maximum in bed elevation is developed in the eddy in both cases, although it develops earlier and is more pronounced in Fig. 8a as a result of the turning of the bottom stress into the eddy.

In Fig. 9, the predicted bed morphology at twenty minute intervals over the entire two hour evolution period is shown for the case with and without secondary flow effects. The deposit in the eddy region grows more rapidly and over a longer period of time in the case with secondary flow effects. If secondary flow effects are neglected, the bed is essentially at equilibrium after about 1 hour, with very little continued erosion or deposition after this period of time. With secondary flow effects, the evolution continues and the bed approaches equilibrium after about two hours, in good agreement with the observed bed evolution. After two hours, the eddy deposit with secondary flows is almost twice the height of the deposit without these effects. In Fig. 10, the predicted cross-section at the position of the maximum eddy bar height is shown along with the measured points from the laboratory experiment. In Fig. 10a, comparison of the predicted and measured bed is reasonably good, with the general shape and elevation of the measured bed well-predicted by the model. In contrast, Fig. 10b shows the same comparison for the case where secondary flow effects are ignored; the model prediction is very poor. We conclude that accurate prediction of

eddy deposition using a physically based model requires incorporation of the secondary flow effects. A more complete comparison of the model results with the measured bathymetry is shown in Figure 11 in the form of contour plots of the predicted and measured bathymetry over the two-meter reach downstream of the separation point where measurements were made. The most obvious deviations between the measurements and the model predictions are found in the main channel. These differences are associated with the passage of small bedforms in the flume experiment that are not treated in the model, which treats bed forms only parametrically through the specification of roughness.

Field Comparison

To test the flow component of the model in a complex field situation, a comprehensive bathymetric surveying and velocity measurement program was carried out at three different lateral separation zones in the Colorado River in Grand Canyon, as described by McDonald and Nelson [in USGS review]. Measurement were made using a profiling array of directional-resolving mechanical current meters in conjunction with a digital compass, and were concentrated along the channelward margin of the lateral separation zones and in the upstream flow channel on the bankward side of the lateral separation zones. Vertical averages computed from these time series of vertical profiles are shown in Fig. 12 along with the predictions of the flow model at the Eminence Break study site (River Mile 44.2) for the discharge at which measurements were made ($\simeq 400 m^3/s$, or 14000 cfs). Both model predictions and measured velocities show typical recirculating flow with the predicted reattachment point in reasonable agreement with the position implied by the bathymetric contours. Both the measurements and the model show that the eddy extends somewhat further upstream along the left (looking downstream) channel bank than one might expect from the planform geometry; this is consistent with site observations and appears to be associated with the rapid crossing of the high-velocity core of the flow from the left bank to the right bank immediately upstream of the study reach. This rapid crossing is driven by a relatively sharp bend in the channel upstream of the study reach. It appears that the model predicts a slightly narrower eddy than the measurements, as can be

seen by noting that, near the center of the channel the model, predicts low-velocity flow directed downstream and into the eddy, while the measurements show stronger turning into the up-river direction at these points. Nevertheless, the overall prediction is reasonable, with the geometry of the eddy, the progressive acceleration in the return channel, and the thin upstream extension of the eddy predicted accurately. The model also predicts a very thin, weak separation eddy on the right-hand side of the channel. Although we did not make measurements in this area, aerial photographs suggest that this may be correct. Considering the topographic complexity of this situation, it appears that the flow model performs adequately.

Unfortunately, field measurements of the evolution of lateral separation deposit over the course of a significant sediment-transporting event with well-documented sediment supply information are unavailable at present. As of this writing, plans for a regulated flood event in the Colorado River in Grand Canyon are being developed, and one of the goals of such a flood would be to obtain the data required for model testing. As the sediment load in this channel is supply limited to at least some degree, and the bed is made up of both sand and bedrock, application of the model requires specification of the initial bed configuration and the upstream sediment supply. Hypothetical computations made assuming that sand covers the bed everywhere and is available in sufficient quantity to assume that loads are determined only by flow competence result in rapid filling of the deep pool in the main channel as well as sedimentation in the eddy. This is primarily a response to the tremendous sediment-transporting capacity of the upstream rapid. Adjusting this inlet supply condition empirically essentially dominates the predictions of the model with regard to deposition rates, so that predictions made without some measured supply are speculative. There are few, if any, situations where the assumption of no supply limitation is valid; application of the bed evolution approach in these situations requires specification of the upstream concentration of suspended load, ideally using measured values.

Conclusions

The model described herein is designed to make accurate predictions of eddy flow and sediment-transport patterns in a wide variety of channel geometries, discharges and sediment supply conditions. In the simple laboratory case discussed above, eddy geometry is determined from the interaction of a small suite of simple processes as evidenced by the fact that, over an wide range of Reynolds number, width-to-depth ratios, and unit discharges, reattachment length is scaled by the expansion width. In natural eddies, this is not true, as externally applied pressure gradient forcing can make a drastic difference in the geometry and flow patterns in eddies. For example, as a heuristic tool consider the simple laboratory eddy discussed above in the case of a curved channel, as shown in Fig. 13. In this case, the pressure field required to steer the flow around the channel bend interacts strongly with the sensitive balance between the pressure field and turbulent diffusion of momentum across the reattachment streamline. In Fig. 13a, where the eddy is located on the inner bank of a channel bend, the pressure field modifications induced by channel curvature cause much more rapid reattachment than found in the straight channel case shown in Fig. 6. On the other hand, when the eddy is on the outer bank of a channel bend, as shown in Fig. 13b, the reattachment length is much longer. This is just one simple example of this kind of effect. Generally, adjustments in eddy length over an order of magnitude can be produced by bank irregularities, downstream channel bars, and channel width variation in the main channel, even for the case when the expansion width is the same. Even for the same bathymetric conditions, variations in discharge can substantially change the pressure field and, through that effect, modify the eddy geometry. For example, in Fig. 14, flow predictions are shown for the Eminence Break site for a discharge of $1200 m^3/s$ ($\simeq 42000$ cfs). The point of reattachment moves significantly downstream relative to the predictions in Fig. 12. This trend continues with increasing discharge, but only up to the point where strong backwater effects begin to occur in response to the lower elevation boundary condition. The complexity of this response, and the general strong interaction between channel morphology and discharge with eddy geometry demonstrates the value of a computational approach to assessing the sediment trapping characteristics of lateral separation eddies.

We believe that the approach taken here is the simplest possible one capable of treating lateral separation zones in rivers in a physically realistic manner. The success of the approach is a result of (1) careful numerical treatment of the full vertically averaged equations, (2) physically realistic specification of lateral and vertical diffusivities, and (3) inclusion of secondary flows. Although the model uses a simple turbulence closure and more sophisticated turbulence closure techniques may yield more accurate results, the additional computational time required renders those approaches difficult to use for bed evolution computations, which typically require on the order of 10^3 iterative flow solutions to be carried out. The method presented here calculates initial flow solutions converged to a very high degree of mass conservation (typically one part in 10^5 at both sections and individual node points) in less than 3 minutes on a Sparcstation 10, and bed evolutions generally take less than one hour of cpu for 1000 time steps, which is sufficient for all but the most dynamic conditions.

The ultimate goal of the model development and testing described in this paper is to employ a well-tested, physically based model to assess the impacts of various flow hydrographs and sediment supply scenarios on deposition and erosion rates in lateral separation eddies both in the Colorado River in Grand Canyon and in other rivers. Two essential elements are required for the success of this undertaking. First, we need a computational model capable of making accurate predictions of eddy flow and sediment transport patterns for a variety of channel geometries and discharges and, second, we need a comprehensive assessment of sediment availability. Obviously, the focus of this paper is on the first of these two elements, but it is extremely important to note that, even given perfect flow computations, this problem is strongly controlled by sediment availability. Preliminary bed evolution results show that, if the main channel concentration falls below a certain level, the loss of sand from the eddy to the main channel will occur for even the highest flow conditions. Thus, accurate predictions of flow are not in themselves sufficient for predicting the behavior of eddy deposits during prescribed flows; sediment availability is at least as important. The next step in the development of the approach described herein is testing of the evolution model for conditions where the initial bed configuration, the discharge history, and the sediment supply are known.

Acknowledgements

This work was supported by the National Research Program of the Water Resources Division of the U.S. Geological Survey, by the Glen Canyon Environmental Studies Program administered by the U.S. Bureau of Reclamation, and by the National Science Foundation (grants CTS-8911359 and CTS-9217804 to S.R. McLean and J.M. Nelson and OCE-8117397 to P.A. Jumars and A.R.M. Nowell). The laser-Dopper velocity measurement program was carried out at the University of Washington Friday Harbor Laboratories. The particle tracking laboratory work was supported by the Civil Engineering Research Institute and the Foundation of the Hokkaido River Disaster Prevention Research Center of the government of Japan. Assistance in the laboratory was provided by E.D. Andrews, D.M. Rubin, S.R. McLean, N. Muneta, and Y. Shimizu.

List of Figures

Figure 1. Schematic diagram of a lateral separation eddy produced by a rectilinear channel expansion.

Figure 2. Time series of cross-stream velocity measured along the reattachment streamline (a) near the surface and (b) near the bed. Mean velocities are marked with arrows along the plot abscissa.

Figure 3. Flow past a lateral obstruction visualized using particle tracking techniques. Flow is from right to left. Raw vectors are shown in (a), while spatially averaged velocities determined from the particle tracks are shown in (b) near the surface and (c) near the bed.

Figure 4. Contours of vertical vorticity (a) and $\frac{\partial w}{\partial z}$ (b) computed from velocity fields determined with video particle tracking.

Figure 5. Computed versus measured vertically averaged streamwise velocity fields for A equal to (a) 0.001, (b) 0.005, (c) 0.01, and (d) 0.02. The flow depth is 0.07m, discharge is 15 l/s, the upstream channel width is 0.35m, and the downstream channel width is 0.70m.

Figure 6. Plots of (a) vertically averaged velocity, (b) vector shear velocity, and (c) surface elevation for the initial conditions of the bed evolution computations: depth is 0.10m, discharge is 22 l/s, and the bed is made up of 0.9mm well-sorted sand. Note that the surface elevation is shown over a longer channel reach than the vertically averaged velocity or shear velocity.

Figure 7. Contours of (a) downstream velocity and (b) cross-stream velocity for the section at the midpoint of the plots shown in Fig. 6a and 6b, for the run conditions given in the caption of Fig. 6.

Figure 8. Contour plots of bed evolution including secondary flow effects (a) and excluding them (b). Starting at the top of the figures, time elapsed since the beginning of bed evolution is 2, 4, 6, 8, 10, and 12 minutes.

Figure 9. Contour plots of bed evolution including secondary flow effects (a) and excluding them (b). Starting at the top of the figures, time elapsed since the beginning of bed evolution is 20, 40, 60, 80, 100, and 120 minutes.

Figure 10. Comparison between measured (symbols) and predicted (solid lines) bed elevation at the section corresponding to the maximum eddy bar elevation for the case with secondary flow effects (a) and without secondary flow effects (b).

Figure 11. Contour plots of computationally predicted (a) and measured evolution contours for the run conditions described in the caption of Fig. 6 after two hours of bed evolution.

Figure 12. Bathymetric contours of the Eminence Break study site with model predictions (black vectors) and flow measurements in the eddy (red arrows).

Figure 13. Vertically averaged velocity vectors computed for simple flat-bedded eddies when the expansion is on the inside of a channel bend (a) and when the expansion is on the outside of the channel bend (b).

Figure 14. Computed vertically averaged velocity vectors for the Eminence Break site at a discharge of $1200 m^3/s$.

References

Bradshaw, P. and F.V.F. Wong, F.V.F., The reattachment and relaxation of a turbulent shear layer, J. Fluid Mech., 52, 113-135, 1972.

Engelund, F. and Hansen, F., A monograph on sediment transport in alluvial streams, in *Teknisk Verlag*, Technical University of Denmark, Copenhagen, Denmark, 66 pp., 1967.

Etheridge, D.W., and Kemp, P.H., Measurements of turbulent flow downstream of a rearward-facing step, J. Fluid Mech. 86, 545-566, 1978.

Hasegawa, K., Hydraulic Research on Planimetric Forms, Bed Topographies and Flow in Alluvial Rivers. Ph.D. Dissertation, Hokkaido University, Sapporo, 1984.

Holton, J.R., *An Introduction to Dynamic Meteorology,* Academic, New York, 1979.

Hooke, R.L., Distribution of sediment transport and shear stresses in a meander bend, J. Geology, 83, 543-565, 1974.

Long, C.E., Wiberg, P.L., and Nowell, A.R.M., Evaluation of von Karman's constant from integral flow parameters, J. Hyd. Eng., 119(10), 1182-1190, 1993.

Mueller, T.J., and Robertson, J.M., A study of the mean motion and turbulence downstream of a roughness element, Modern Developments in Theor. Appl. Mech., 1, 326-340, 1963.

Neary, V.S., and A.J. Odgaard, Three-dimensional flow structure at open-channel diversions, J. Hyd. Eng., 119(11), 1223-1230, 1993.

Neary. V.S., Barkdoll, B., and Odgaard, A.J., Sandbar formation in side-diversion channels, Proceedings Of the National Conference, Hydraulics Division, ASCE, Buffalo, New York, 1171-1175, 1994.

Nelson, J.M., and Smith, J.D., Flow in meandering channels with natural topography, in: S. Ikeda and G. Parker (eds), *River Meandering*, AGU Water Resources Monograph 12, Washington, D.C., p. 69-102, 1989.

Nelson, J.M., and Smith, J.D., Evolution and stability of erodible channel beds, in: S. Ikeda and G. Parker (eds), *River Meandering*, AGU Water Resources Monograph 12, Washington, D.C., p. 321-377, 1989.

Nelson, J.M., Experimental and theoretical investigation of lateral separation eddies: Eos Transactions, American Geophysical Union, v. 72(44), p. 218, 1991.

Nelson, J.M., McDonald, R.R., and Rubin, D.M., Flow and sediment transport in lateral separation eddies, submitted.

Patankar, S.V., and Spalding, D.B., *Heat and Mass Transfer in Boundary Layers,* Intertext, London, 1970.

Patankar, S.V., *Numerical Heat Transfer and Fluid Flow,* Hemisphere, New York, 1980.

Ponce, V.M., and Yabusaki, S.B., J. Hyd. Eng., 107, 1501-1518, 1981.

Press, W.H., Flannery, B.P., Teukolsky, S.A., and Vetterling, W.T., *Numerical Recipes: The Art of Scientific Computing,* Cambridge Press, New York, 1986.

Rattray, M. Jr., and Mitsuda, E., Theoretical analysis of conditions in a salt wedge, Estuarine, Coastal, and Marine Science, 2, 373-394, 1974.

Rodi, W., *Turbulence Models and Their Application in Hydraulics,* 104 pp., International Association for Hydraulic Research, Delft, 1980.

Rozovskii, I.L., *Flow of Water in Bends of Open Channels,* 233 pp., Israel Program for Scientific Translation, originally published by Academy of Sciences of the Ukrainian SSR, Kiev, 1957.

Rubin, D.M., Schmidt, J.C., and Moore, J.N., Origin, structure and evolution of a reattachment bar, Colorado River, Grand Canyon, Arizona, Journal of Sedimentary Petrology, 60, 982-991, 1990.

Schlichting, H., *Boundary Layer Theory,* 817 pp., McGraw-Hill, New York, 1979.

Schmidt, J.C., Recirculating flow and sedimentation in the Colorado River in Grand Canyon, Arizona, Journal of Geology, 98, 709-724, 1990.

Schmidt, J.C., Rubin, D.M., and Ikeda, H., Flume simulation of recirculating flow and sedimentation, Water Resources Res., 29, 2925-2939, 1993.

Shimizu, Y., Smith, J.D., and Nelson, J.M., 1989, Comparison of models for single thread streams, in: S.Y. Wang (ed), Proceedings of the International Symposium on Sediment Transport Modeling, ASCE, New York, p. 524-529.

Simpson, R.L., Turbulent boundary-layer separation, Ann. Rev. Fluid Mech., 21, 205-234, 1989.

Smith, J.D., and S.R. McLean, Spatially averaged flow over a wavy surface, J. Geophysical Research, v. 82, 1735-1746, 1977.

Smith, J.D., and S.R. McLean, A model for flow in meandering streams, Water Resour. Res., 20(9), 1301-1315, 1984.

Tani, I., Experimental investigation of flow separation over a step, in *Boundary Layer Research* (ed. Gortler, H.), 377-386, Springer-Verlag, Berlin, 1958.

Tennekes, H., and Lumley, J.L., *A First Course in Turbulence,* 300 pp., MIT Press, Cambridge, Mass., 1972.

Wiberg, P.L., and J.D. Smith, A theoretical model for saltating grains in water, J. Geophysical Res., 90(4), 7341-7354, 1985.

Yalin, M.S., An expression for bedload transportation, J. Hydraul. Div. ASCE, 89(HY3), 221-250, 1963.

Yeh, H.H., Chu, W., and Dahlberg, O., Numerical modeling of separation eddies in shallow water, Water Resources Res., 24, 607-614, 1988.

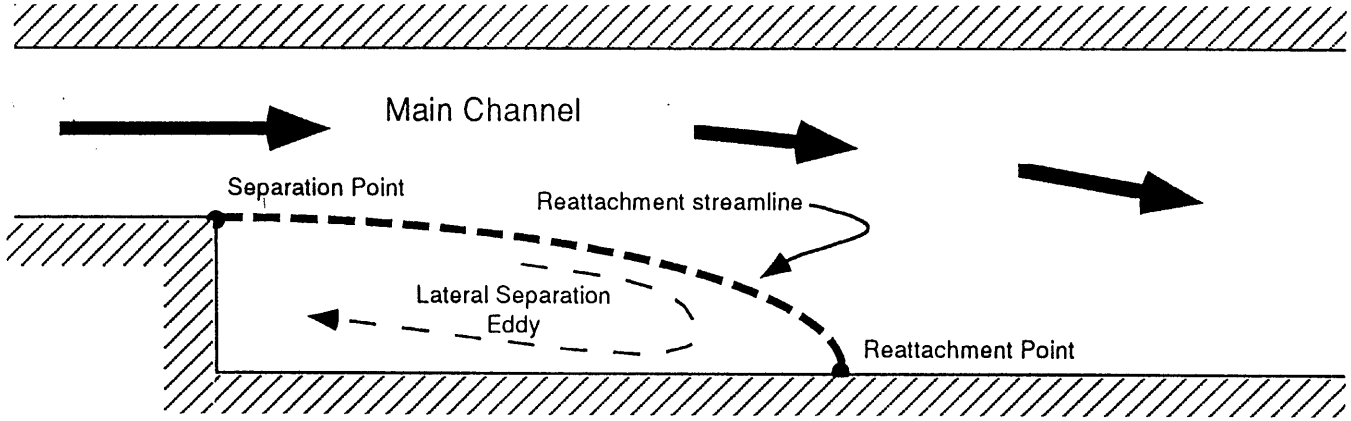
Main Channel
Separation Point
Reattachment streamline
Lateral Separation
Eddy
Reattachment Point

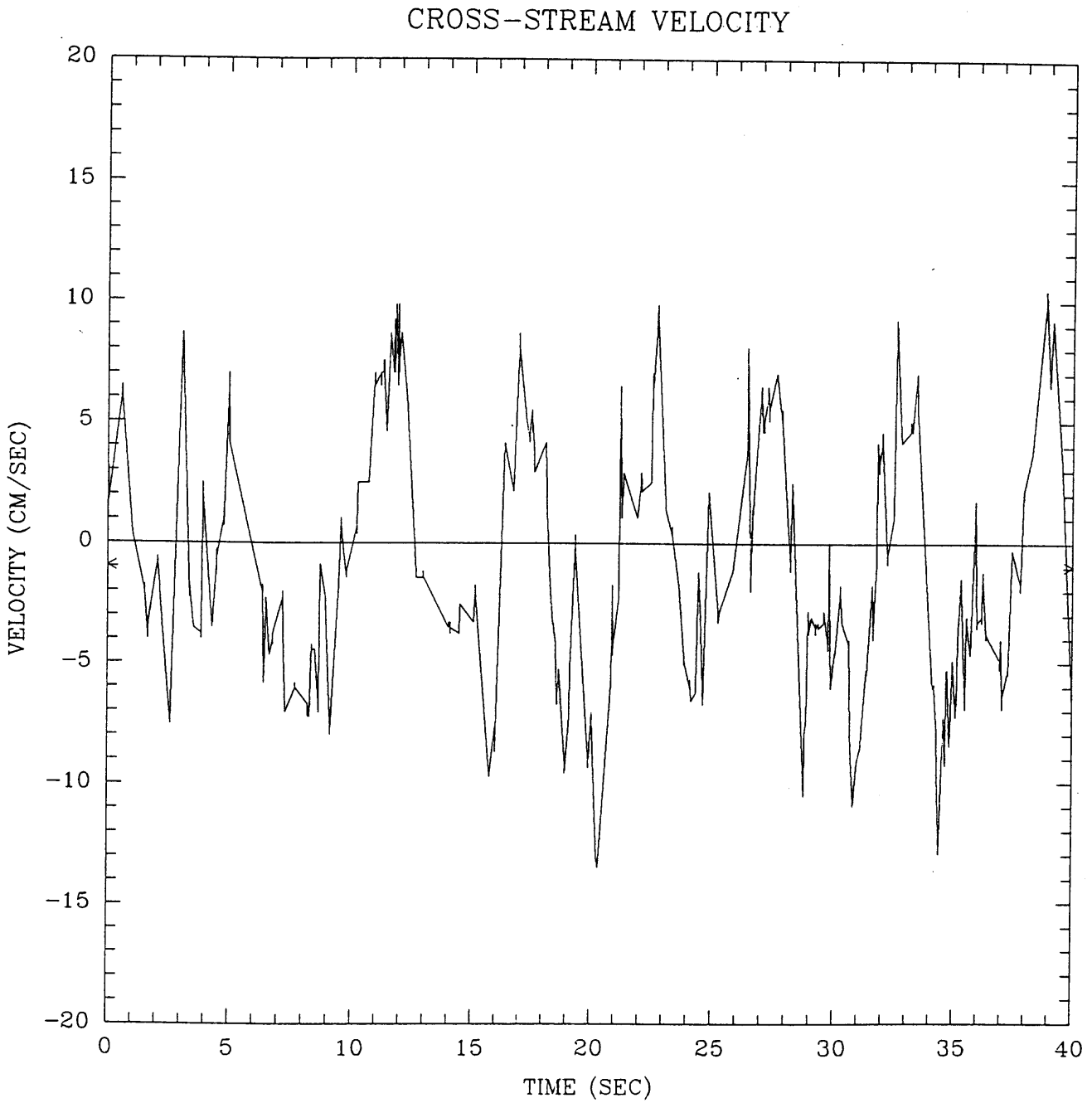
CROSS-STREAM VELOCITY
VELOCITY (CM/SEC)
TIME (SEC)
20
15
10
5
0
-5
-10
-15
-20
0
5
10
15
20
25
30
35
40

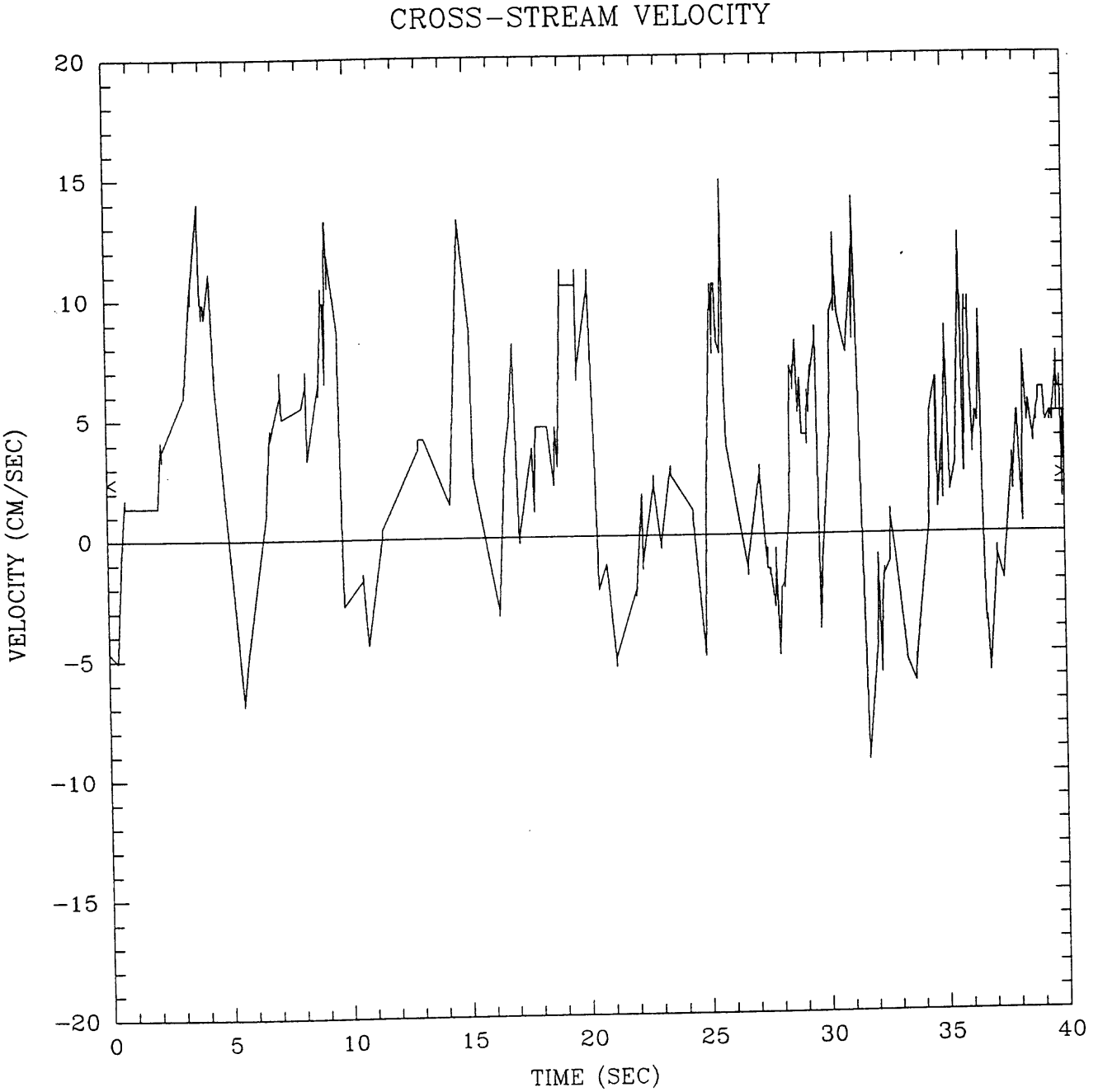
CROSS-STREAM VELOCITY
VELOCITY (CM/SEC)
TIME (SEC)
20
15
10
5
0
-5
-10
-15
-20
0
5
10
15
20
25
30
35
40

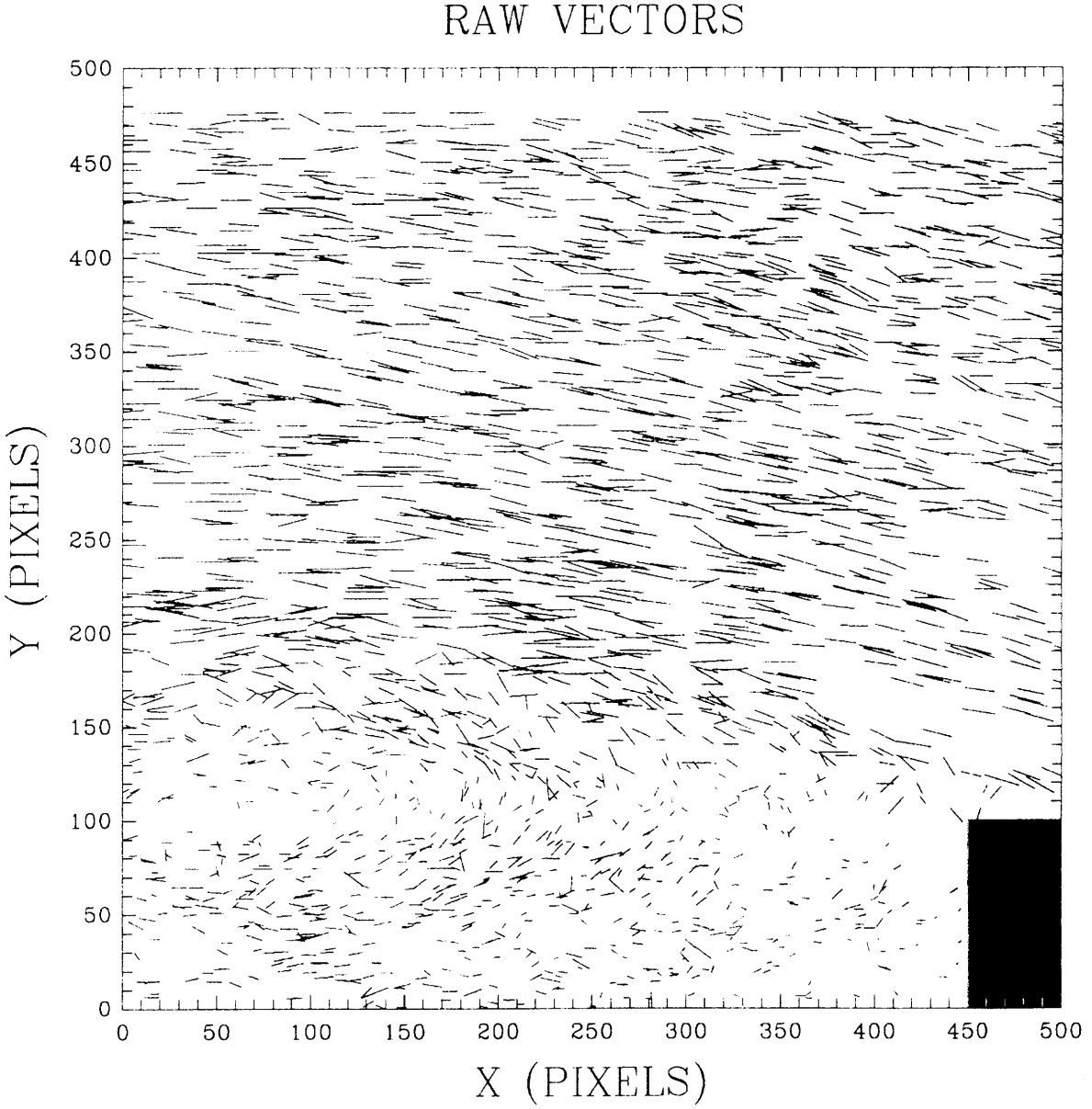
RAW VECTORS
Y (PIXELS)
X (PIXELS)
0
50
100
150
200
250
300
350
400
450
500

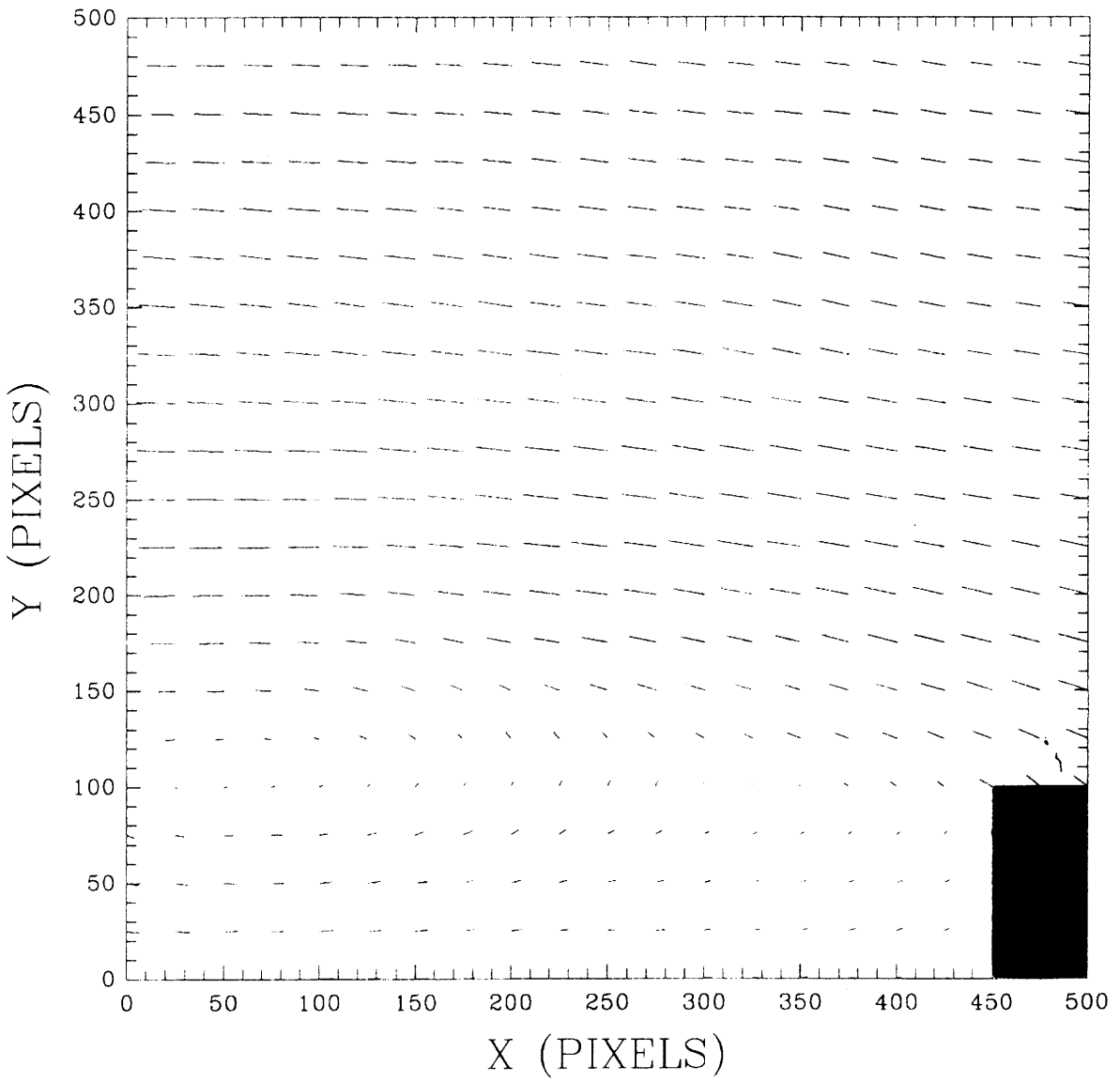
INTERPOLATED VECTORS
Y (PIXELS)
X (PIXELS)
0
50
100
150
200
250
300
350
400
450
500

Fig 3b

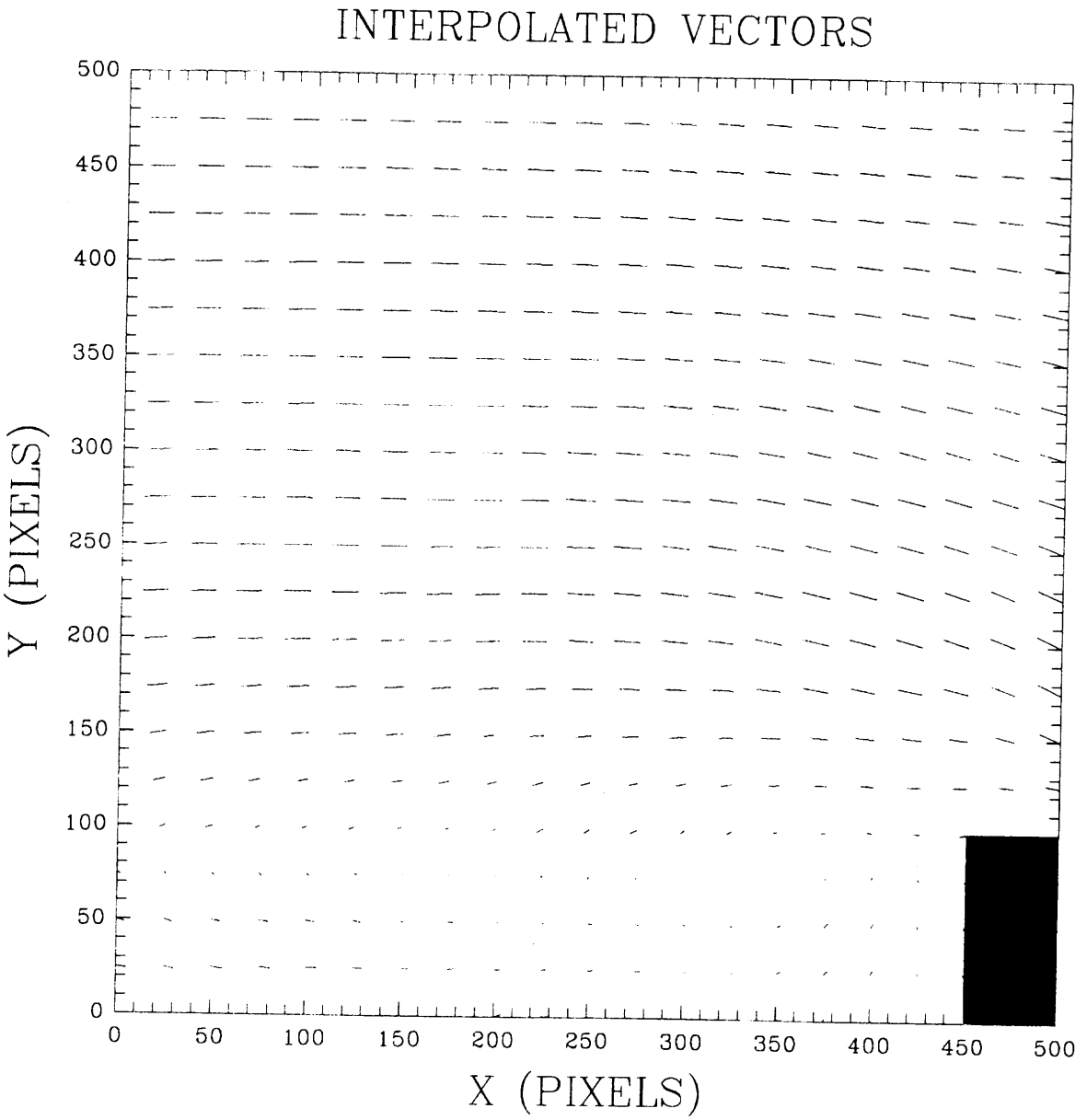
INTERPOLATED VECTORS
Y (PIXELS)
X (PIXELS)
500
450
400
350
300
250
200
150
100
50
0
0
50
100
150
200
250
300
350
400
450
500

Fig. 3c

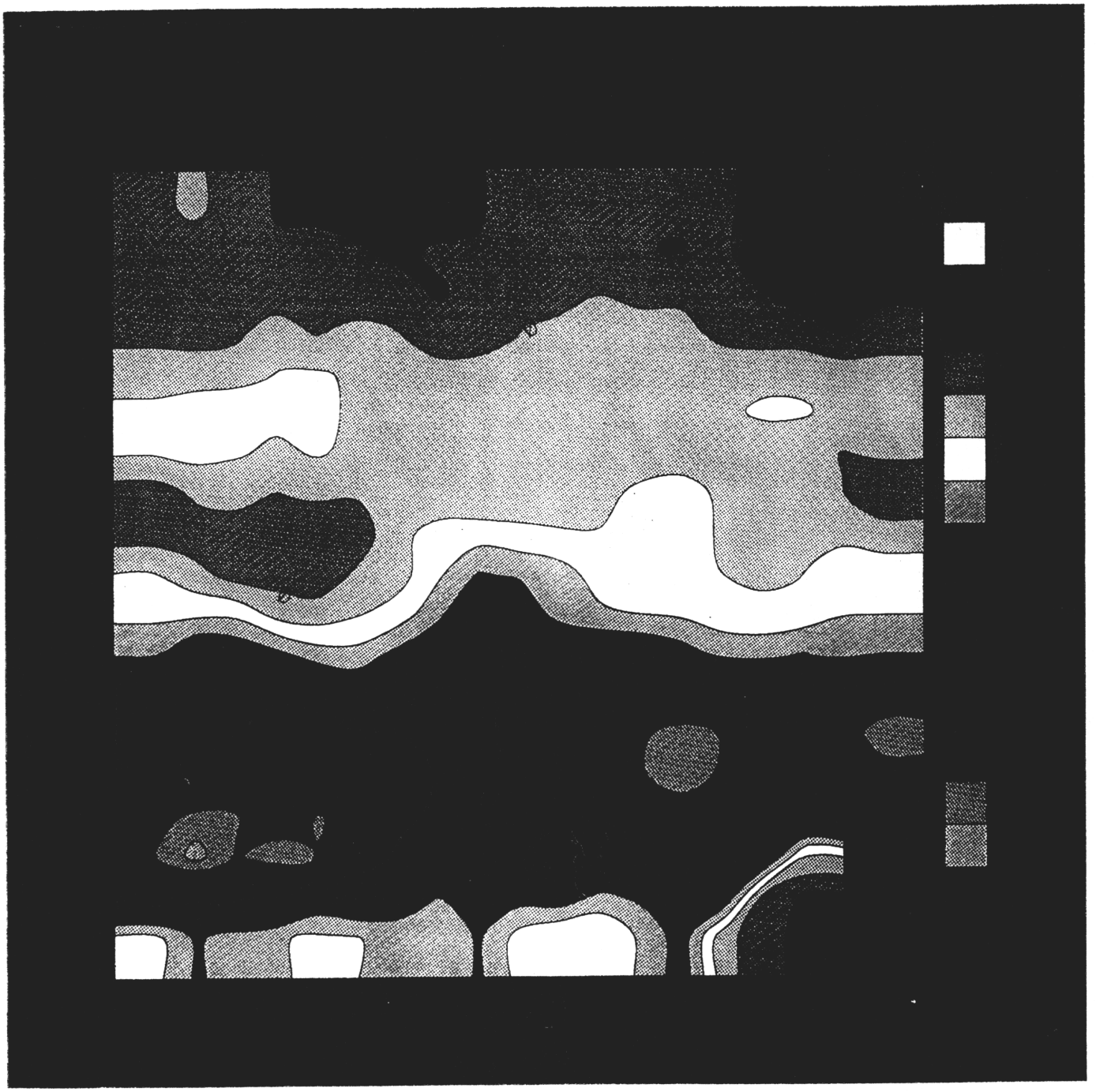

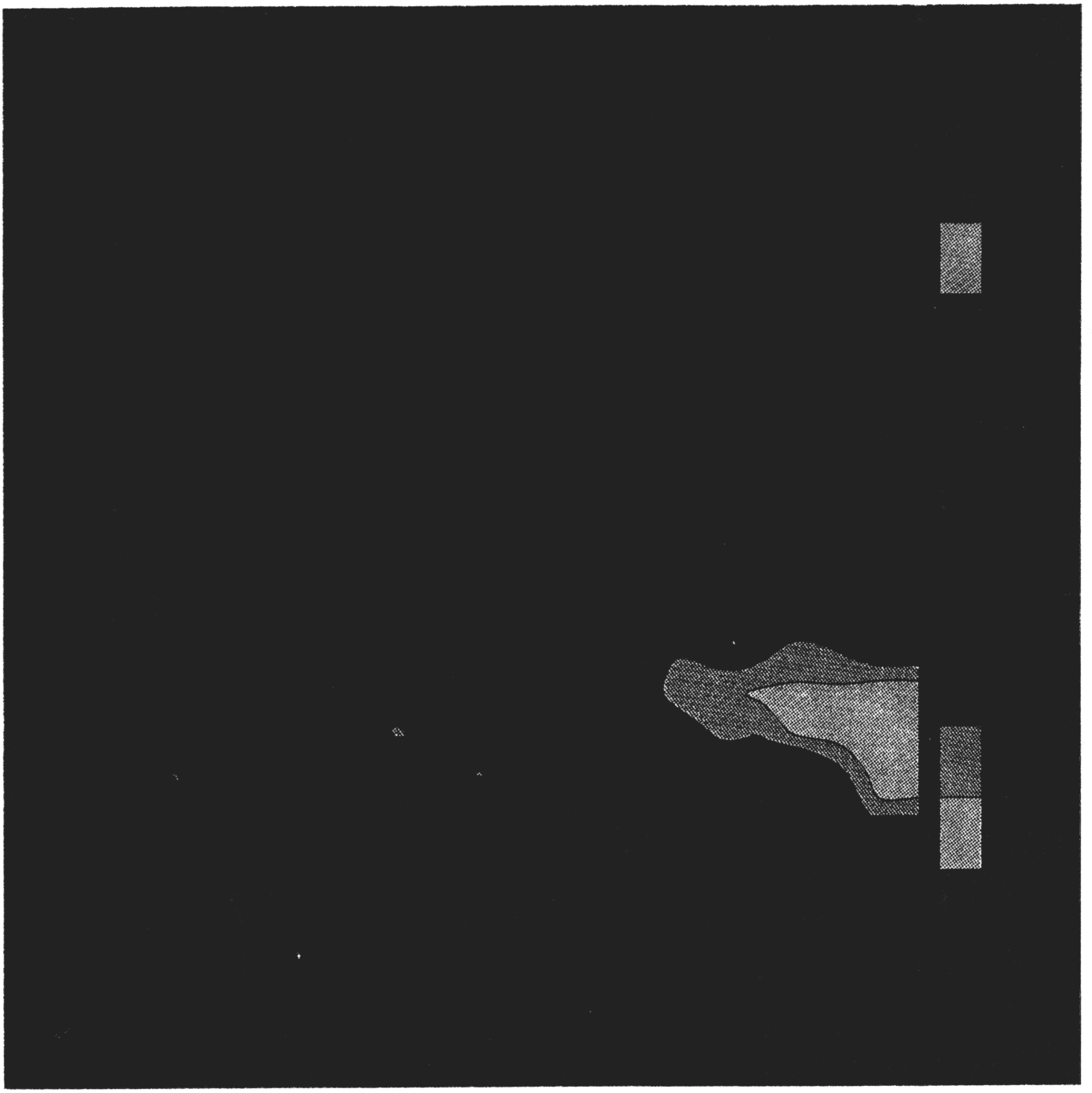

Vertically–averaged velocity for exp 1

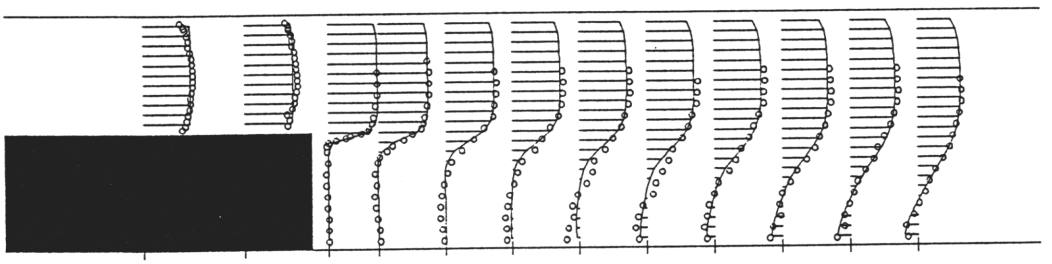

—— MAXIMUM VELOCITY IS 62. CM/SEC

Vertically–averaged velocity for exp 1

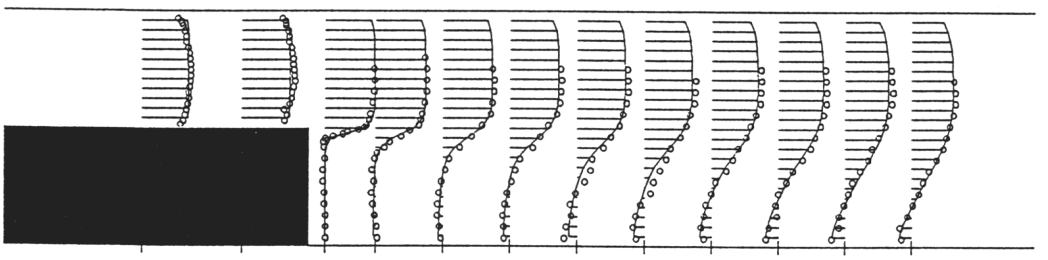

—— MAXIMUM VELOCITY IS 63. CM/SEC

Vertically–averaged velocity for exp 1

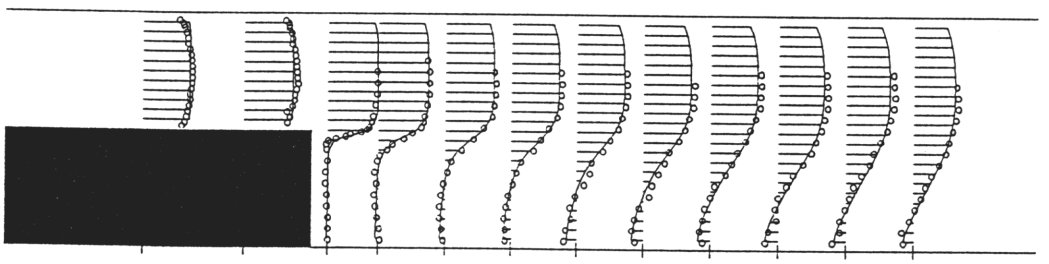

—— MAXIMUM VELOCITY IS 63. CM/SEC

Vertically–averaged velocity for exp 1

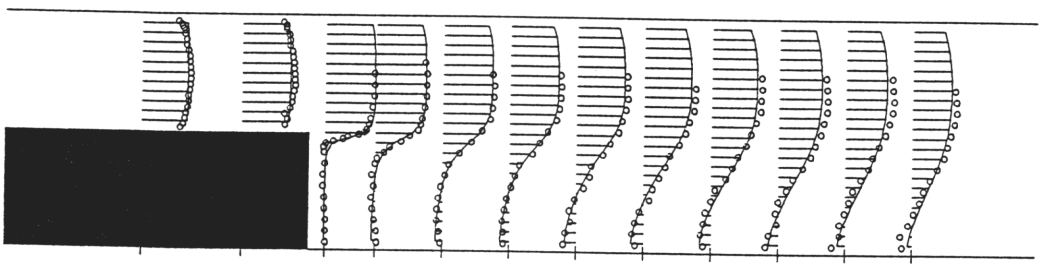

—— MAXIMUM VELOCITY IS 63. CM/SEC

FIG 5D

Vertically-averaged velocity for exp 1

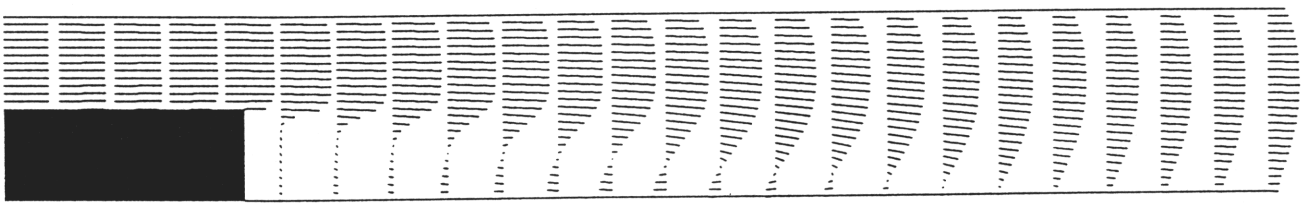

—— MAXIMUM VELOCITY IS 63. CM/SEC

Vector shear velocity for exp 1

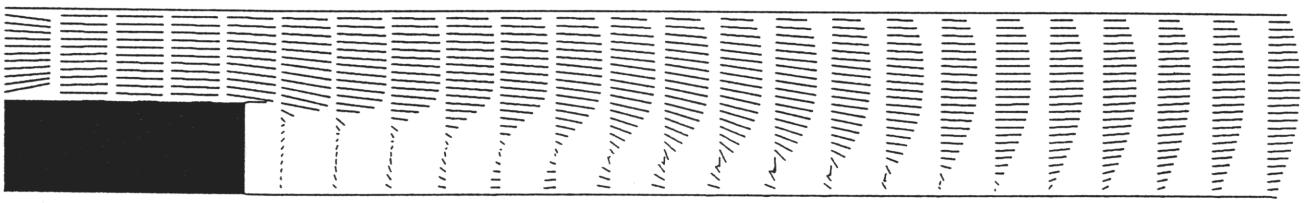

—— MAXIMUM SHEAR VELOCITY IS 7. CM/SEC

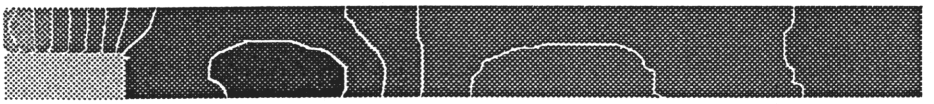

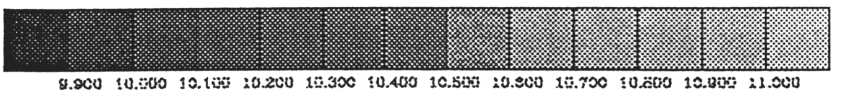
9.900 10.000 10.100 10.200 10.300 10.400 10.500 10.600 10.700 10.800 10.900 11.000

FIG 6C

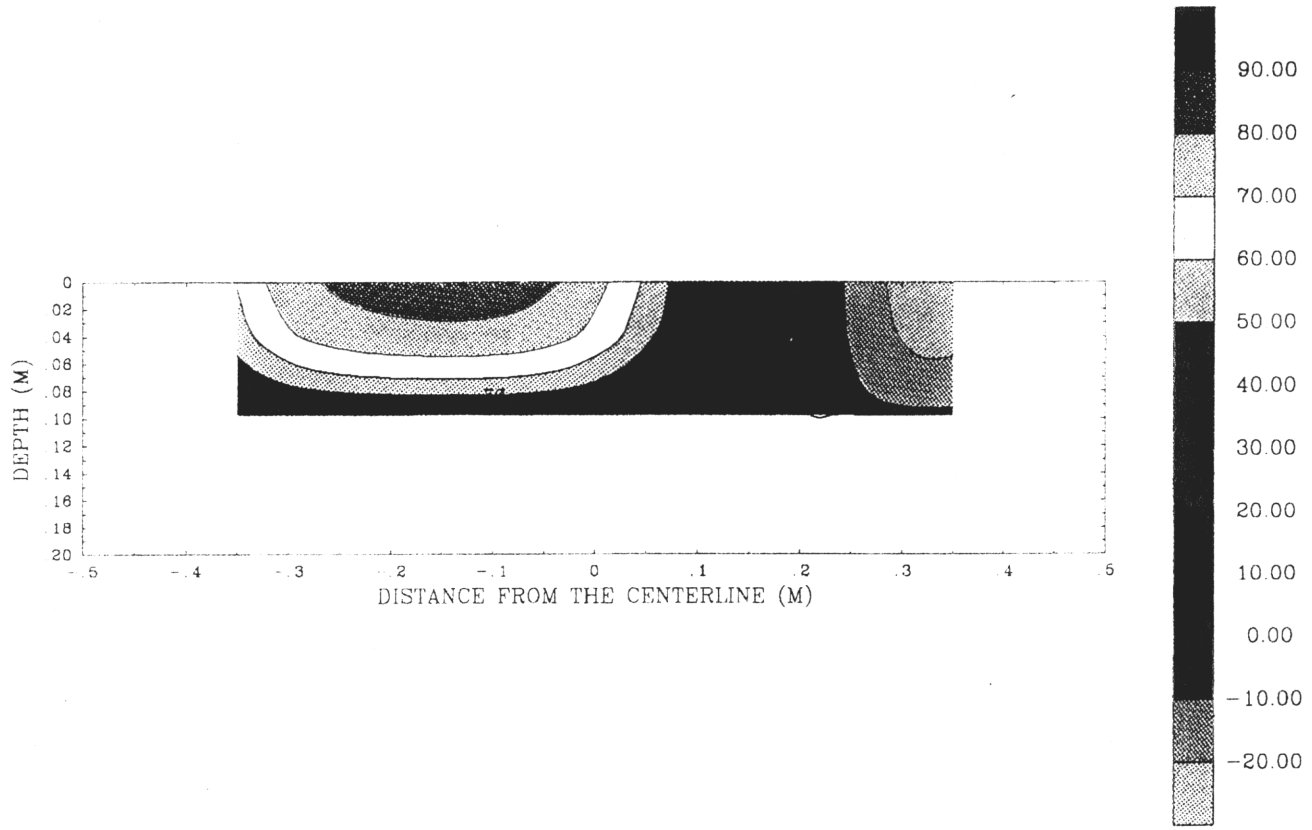
DEPTH (M)
0
02
04
06
08
10
12
14
16
18
20
-.5
-.4
-.3
-.2
-.1
0
.1
.2
.3
.4
.5
DISTANCE FROM THE CENTERLINE (M)
90.00
80.00
70.00
60.00
50.00
40.00
30.00
20.00
10.00
0.00
-10.00
-20.00

Fig 7A

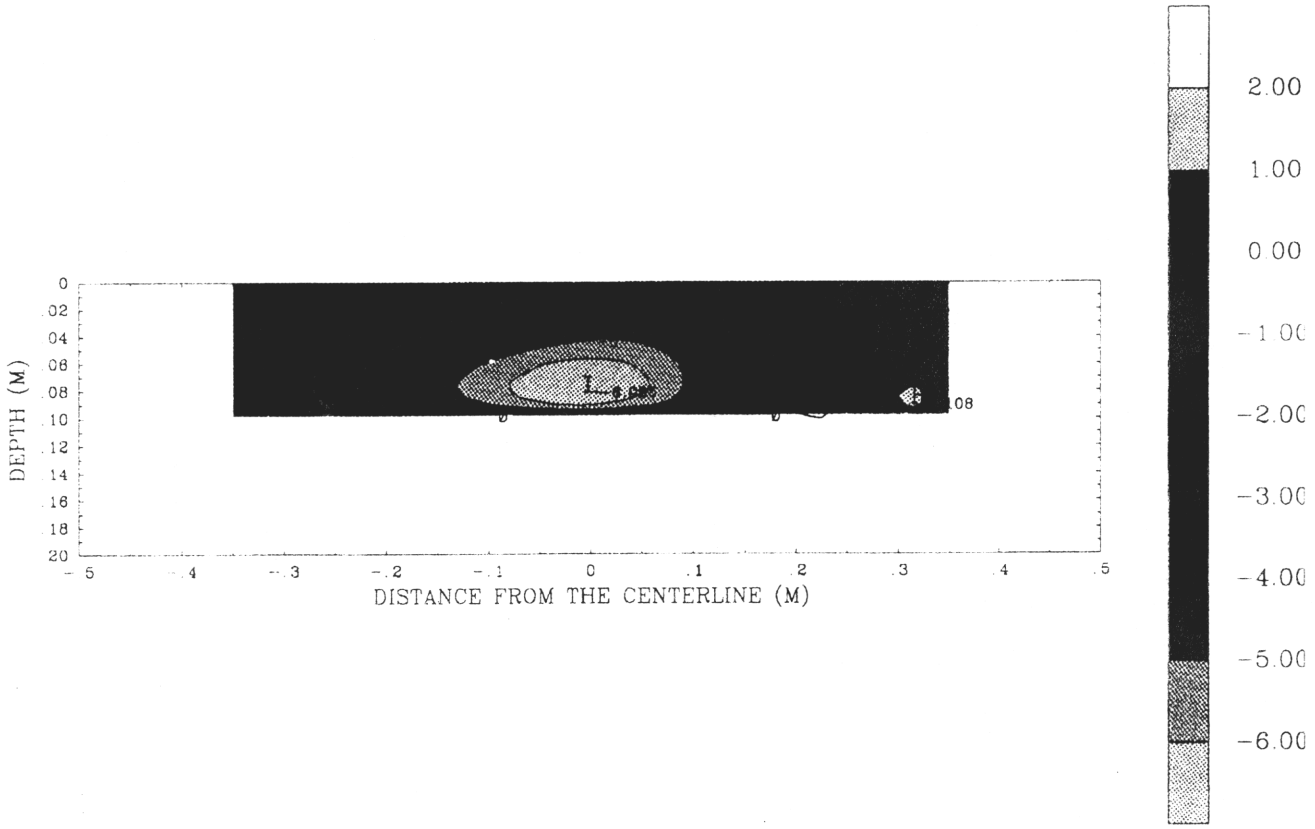
2.00
1.00
0.00
-1.00
-2.00
-3.00
-4.00
-5.00
-6.00
DEPTH (M)
0
.02
.04
.06
.08
.10
.12
.14
.16
.18
.20
-.5
-.4
-.3
-.2
-.1
0
.1
.2
.3
.4
.5
DISTANCE FROM THE CENTERLINE (M)

FIG 7B

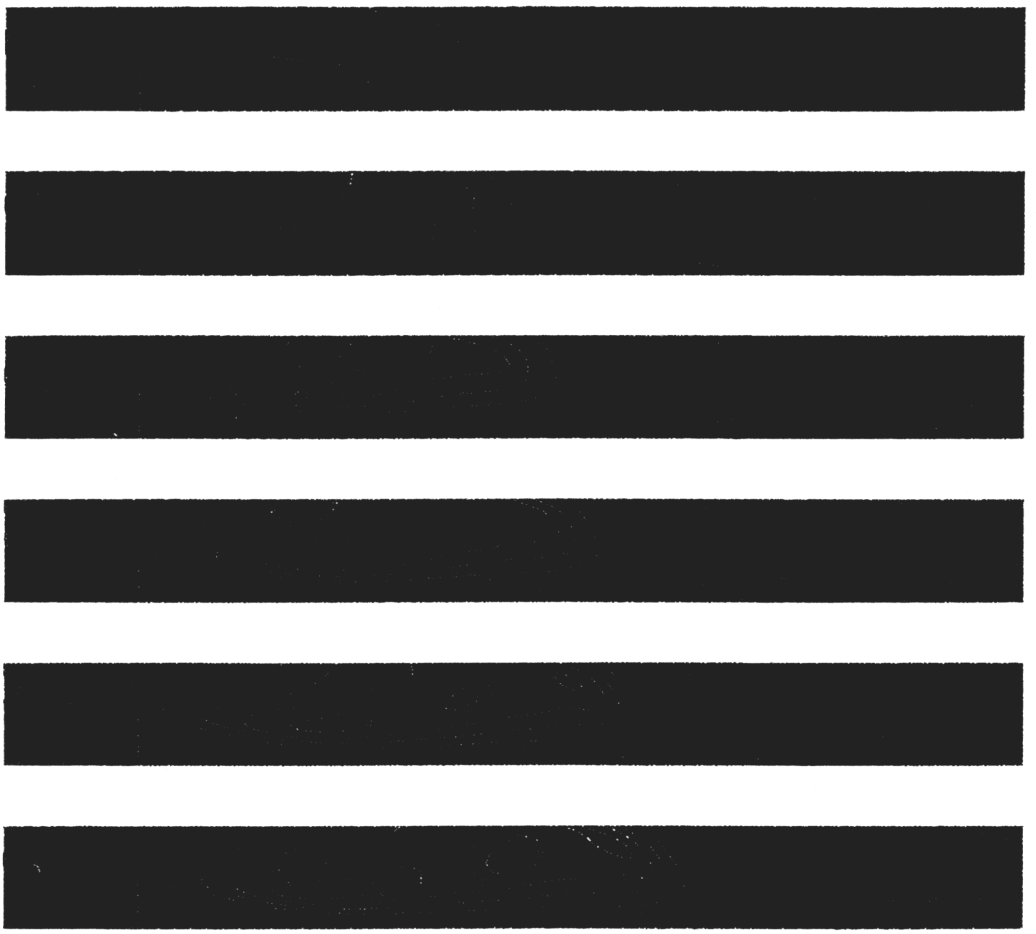

Fig 8A

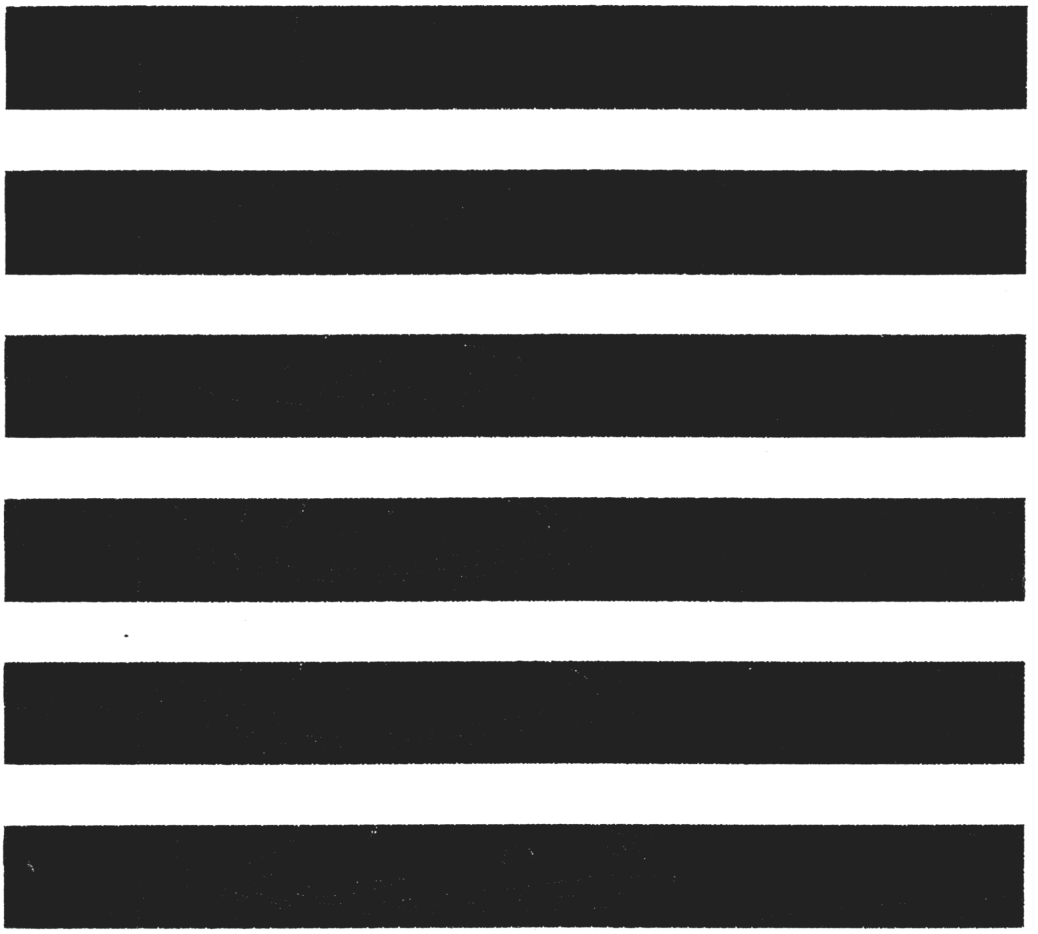

F14 8 B

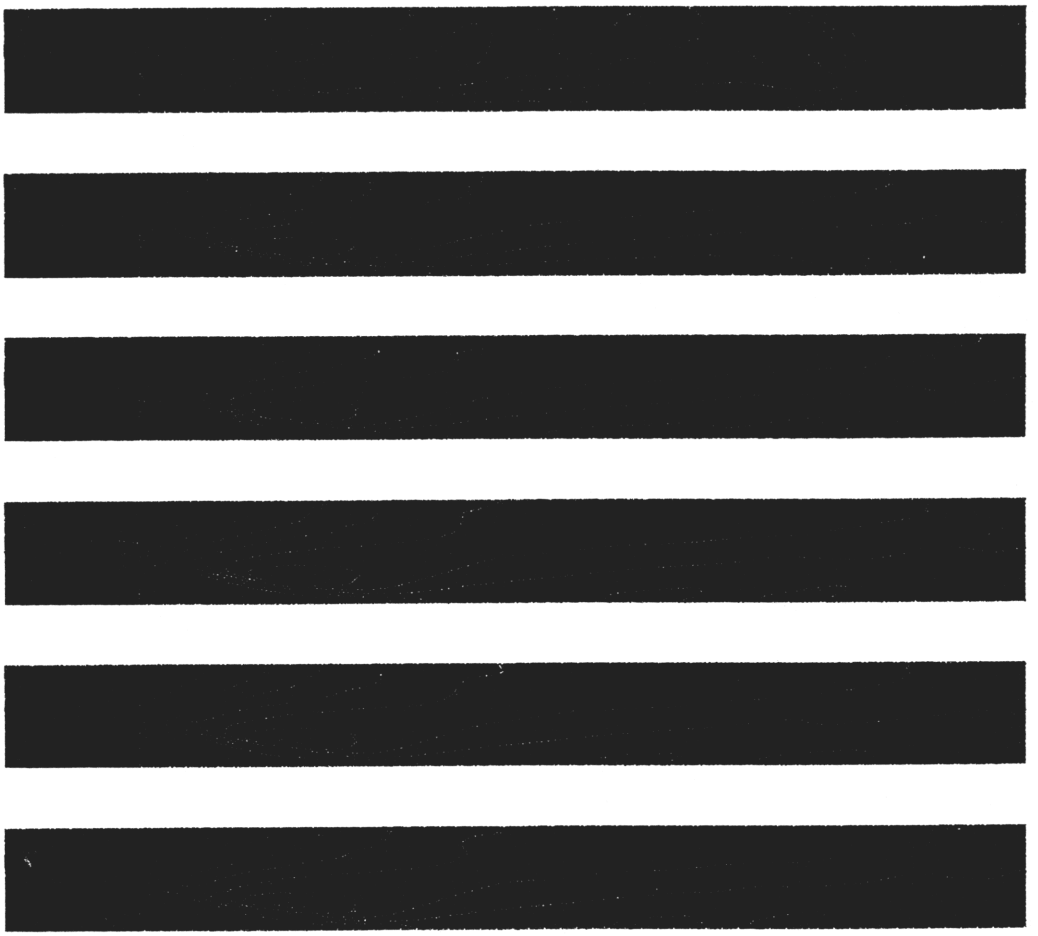

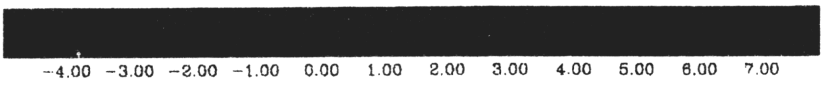

Fig 9A

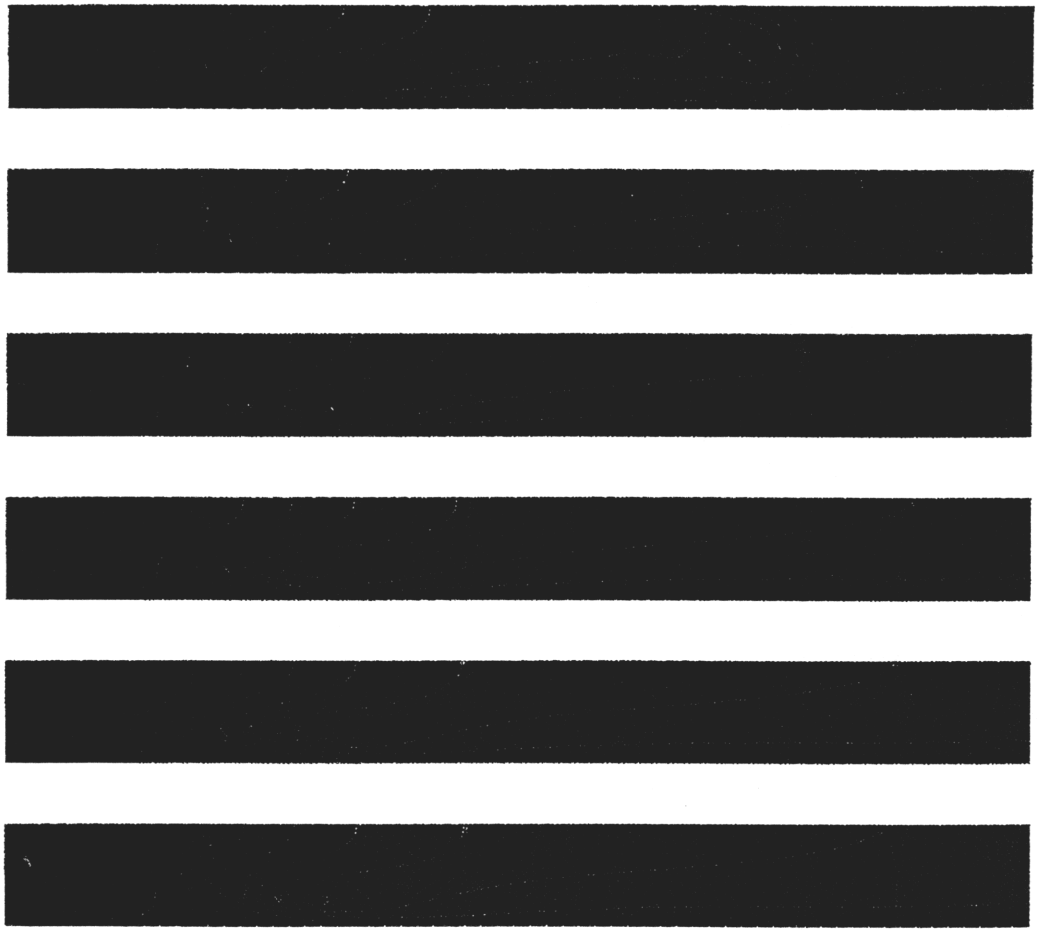

Fig 9R

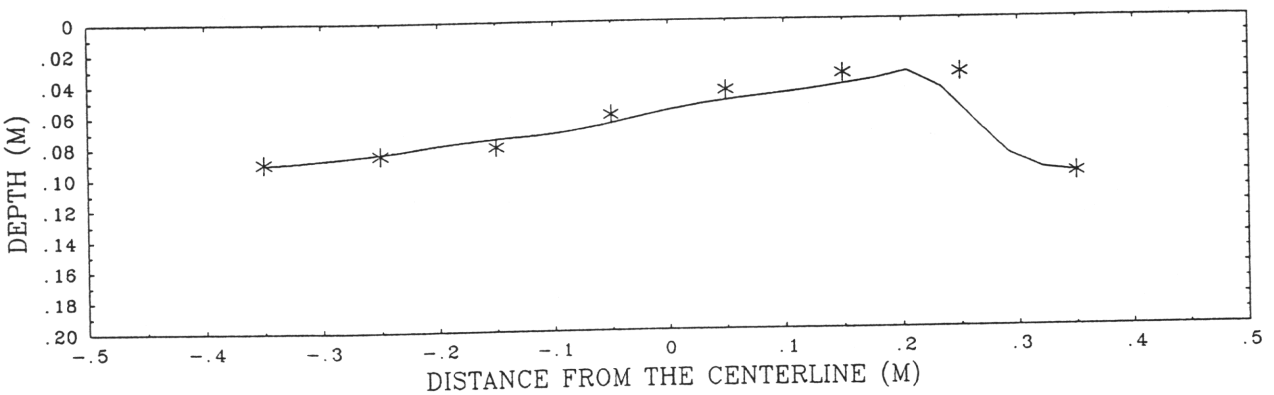
0
.02
.04
.06
.08
.10
.12
.14
.16
.18
.20
DEPTH (M)
-.5
-.4
-.3
-.2
-.1
0
.1
.2
.3
.4
.5
DISTANCE FROM THE CENTERLINE (M)

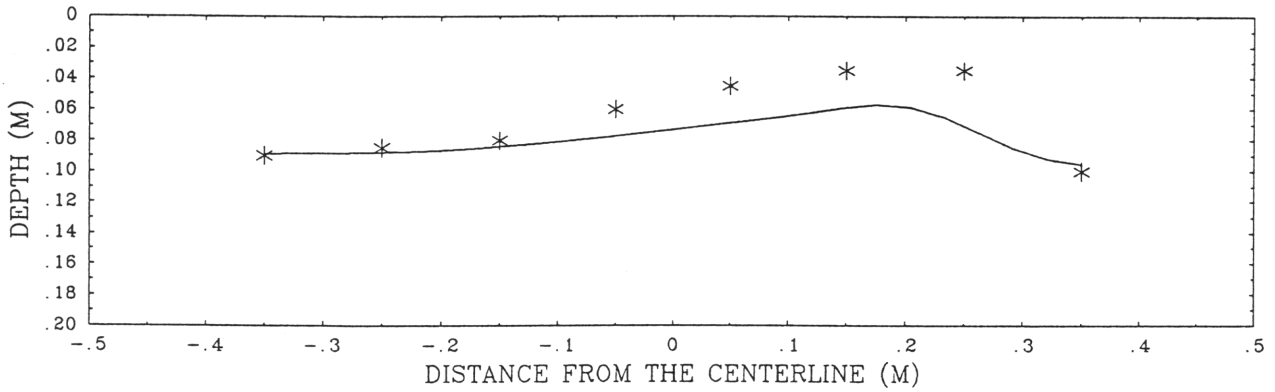
0
.02
.04
.06
.08
.10
.12
.14
.16
.18
.20
DEPTH (M)
−.5
−.4
−.3
−.2
−.1
0
.1
.2
.3
.4
.5
DISTANCE FROM THE CENTERLINE (M)

FIL 10 P

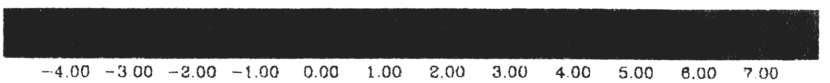
-4.00 -3.00 -2.00 -1.00 0.00 1.00 2.00 3.00 4.00 5.00 6.00 7.00

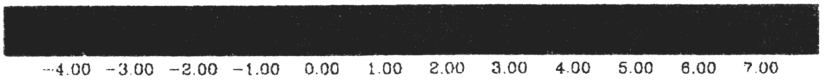

FIG 113

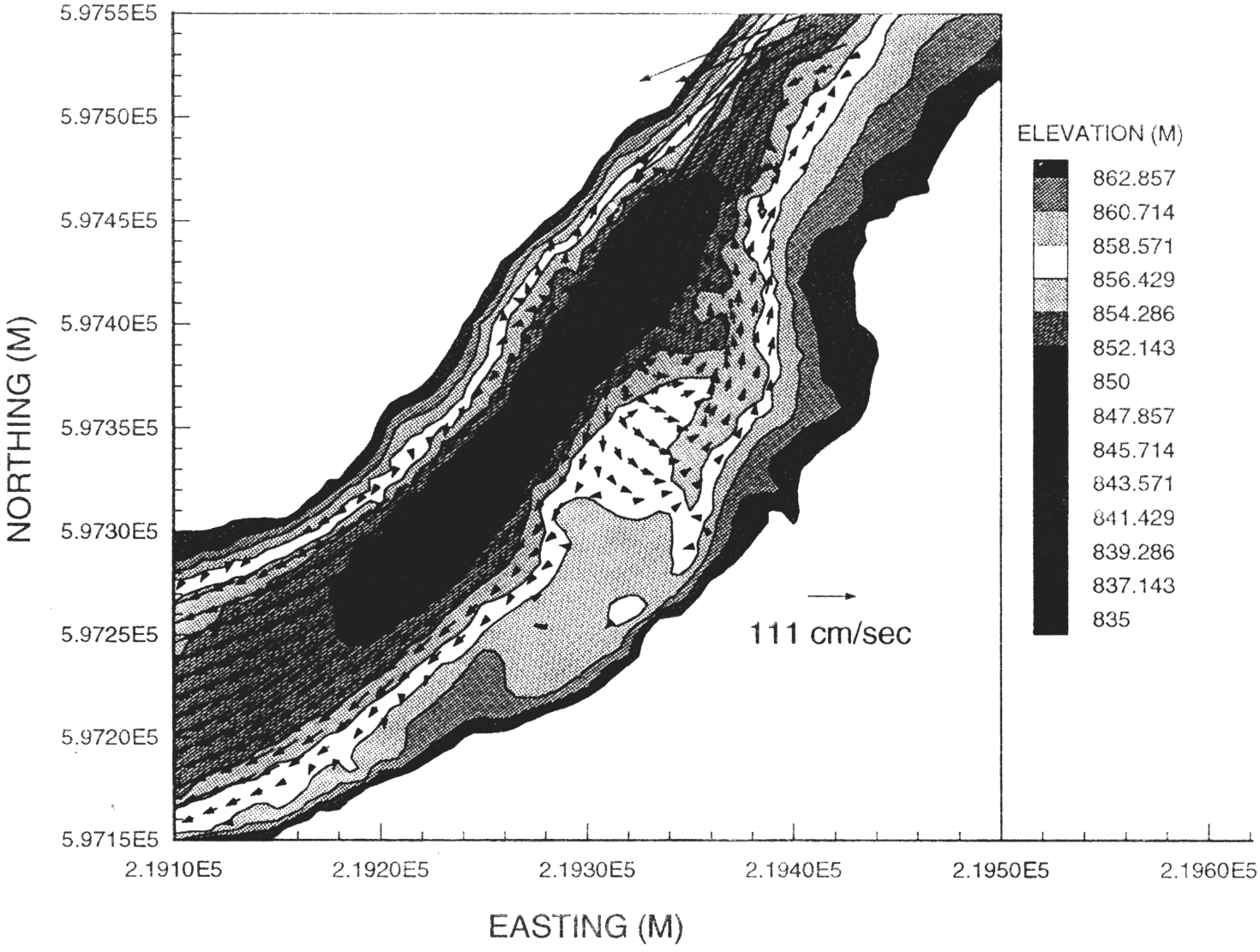
5.9755E5
5.9750E5
5.9745E5
5.9740E5
5.9735E5
5.9730E5
5.9725E5
5.9720E5
5.9715E5
NORTHING (M)
2.1910E5
2.1920E5
2.1930E5
2.1940E5
2.1950E5
2.1960E5
EASTING (M)
ELEVATION (M)
862.857
860.714
858.571
856.429
854.286
852.143
850
847.857
845.714
843.571
841.429
839.286
837.143
835
111 cm/sec

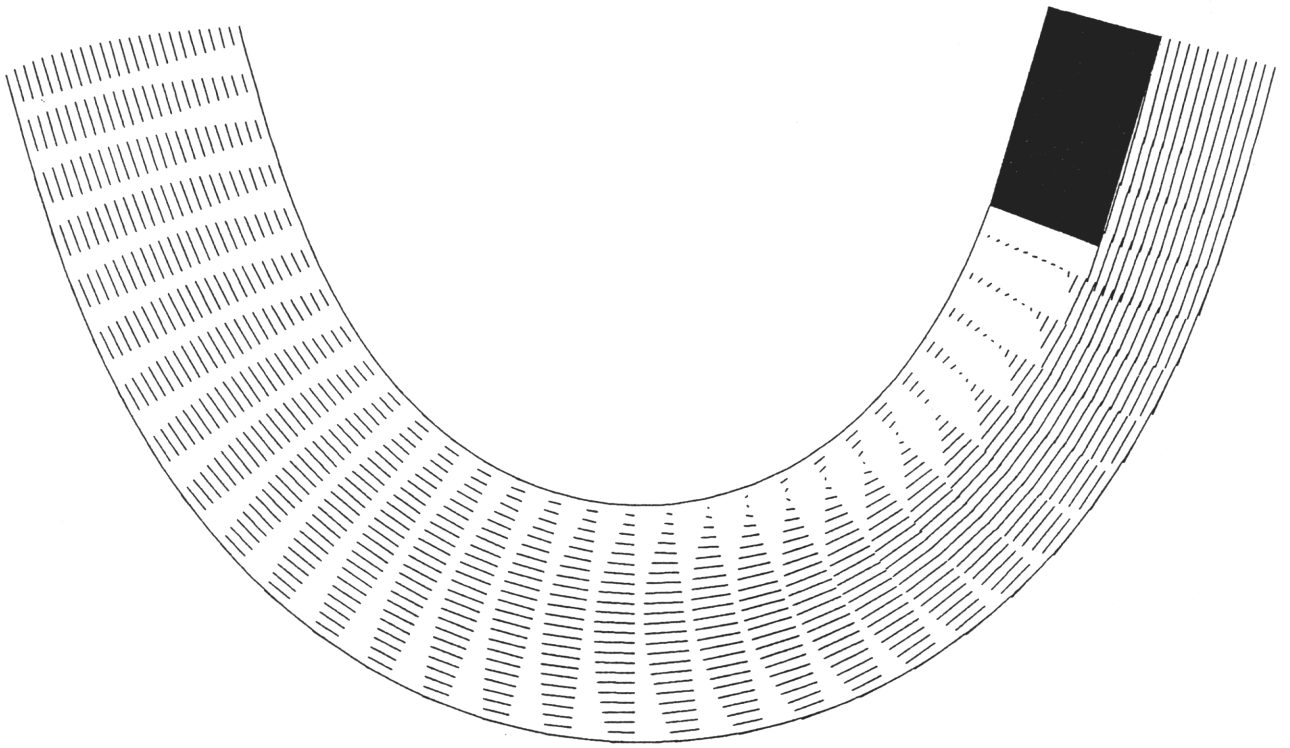

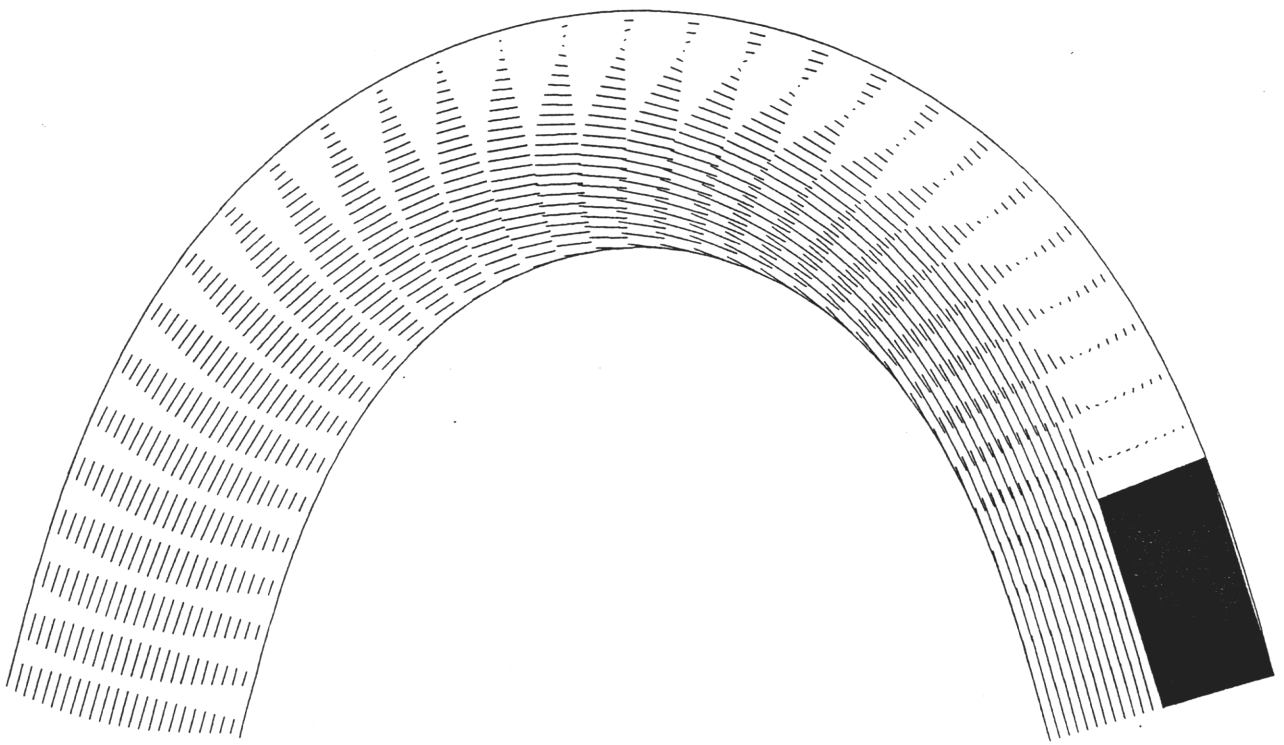

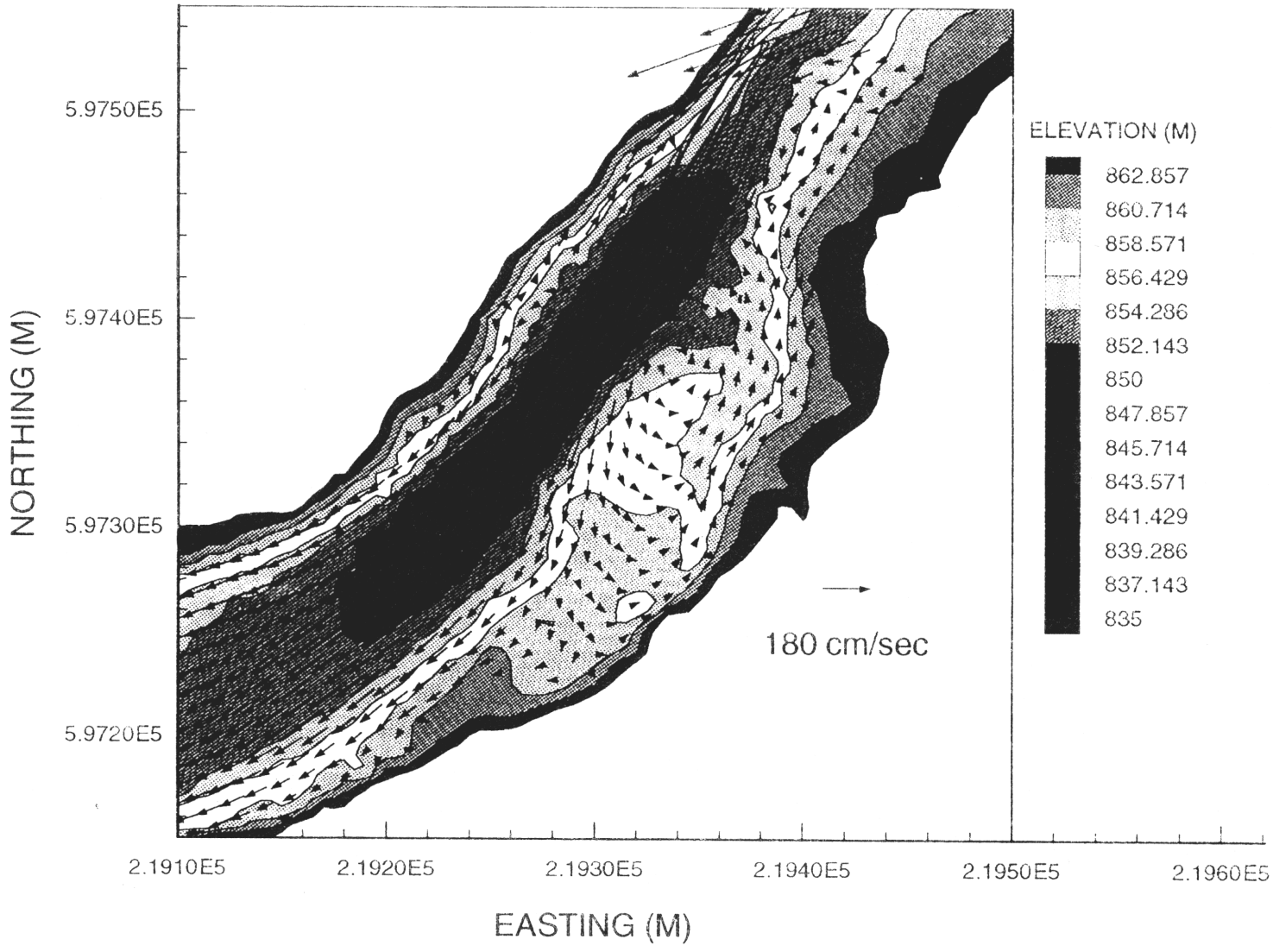
5.9750E5
5.9740E5
5.9730E5
5.9720E5
NORTHING (M)
ELEVATION (M)
862.857
860.714
858.571
856.429
854.286
852.143
850
847.857
845.714
843.571
841.429
839.286
837.143
835
180 cm/sec
2.1910E5
2.1920E5
2.1930E5
2.1940E5
2.1950E5
2.1960E5
EASTING (M)